JOURNAL OF PETROLOGY | VOLUME 50 | NUMBER 10 | PAGES 1899–1933 | 2009 | doi:10.1093/petrology/egp056

Origin of Nepheline-normative High-K Ankaramites and the Evolution of Eastern Srednogorie Arc in SE Europe

S. GEORGIEV[1]*, P. MARCHEV[2], C. A. HEINRICH[1], A. VON QUADT[1], I. PEYTCHEVA[1,2] AND P. MANETTI[3]

[1]INSTITUTE OF ISOTOPE GEOLOGY AND MINERAL RESOURCES, ETH ZURICH, CLAUSIUSSTRASSE 25, CH-8092 ZURICH, SWITZERLAND

[2]GEOLOGICAL INSTITUTE, BULGARIAN ACADEMY OF SCIENCES, ACAD. G. BONCHEV ST., 1113 SOFIA, BULGARIA

[3]DIPARTIMENTO DI SCIENZE DELLA TERRA, UNIVERSITÀ DEGLI STUDI DI FIRENZE, VIA LA PIRA, 4, I-50121, FIRENZE, ITALY

RECEIVED JULY 30, 2008; ACCEPTED JULY 29, 2009

Eastern Srednogorie is part of the Apuseni–Banat–Timok–Srednogorie magmatic belt in SE Europe, the main arc related to the Late Cretaceous subduction and closure of the Tethys Ocean between Africa and Europe. Extrusive and shallow intrusive magmatism in the Eastern Srednogorie is abundant and extremely diverse in composition, covering a wide range from ultramafic volcanic rocks to granites; this provides a unique opportunity to study processes of primitive melt formation and magma evolution in an arc environment. In contrast to other parts of the belt, relatively mafic lavas predominate here. Three magmatic regions are distinguished within Eastern Srednogorie from south to north: Strandzha, Yambol–Burgas and East Balkan. Systematic differences exist between these regions, notably the increased alkalinity of samples from the Yambol–Burgas region in the central part. All rocks display a clear subduction-like signature in their trace-element patterns, particularly the enrichment in large ion lithophile elements and light rare earth elements relative to high field strength elements. A distinct primitive nepheline-normative ankaramite magma type is recognized among the mafic volcanic rocks from the Yambol–Burgas region and melt inclusions entrapped in olivine and clinopyroxene from a cumulitic rock. Lower crustal clinopyroxene and amphibole cumulates carried to the surface as xenoliths in a mafic dike represent a possible source for the ankaramite. Modeling of the melting process suggests that low degrees of batch melting of a clinopyroxene-rich, amphibole-bearing source similar to the cumulate xenoliths at 1 GPa, temperatures of 1240–1300°C, oxidized conditions and a water content of 0·2 wt % reproduce accurately most of the observed major- and trace-element characteristics of the studied ankaramites. The elevated Rb, K_2O, Th, Ba content and higher Pb isotope ratios of the predicted liquids compared with the ankaramites are explained by mixing of the ankaramite magma with lherzolite partial melts derived from the subduction-modified mantle wedge. Underplating of such mantle-derived magmas at the crust–mantle boundary in an extensional environment as a response to slab roll-back provides also the necessary heat to melt lower crustal cumulates. Fractional crystallization of mainly clinopyroxene plus olivine and Fe–Ti oxides in a deep (equivalent to 8 kbar pressure) magma chamber produced most of the observed range of shoshonitic basalts and basaltic andesites in Eastern Srednogorie. The more evolved intermediate varieties were probably formed by mixing and crystallization at lower temperatures in lower pressure magma chambers. Whole-rock Sr and Pb isotope compositions indicate variable degrees of admixing of basement rocks to generate the intermediate to acid Late Cretaceous magmas, but assimilation was minimal for magmas with less than 53 wt % SiO_2. The proposed model for the evolution of the magmatism in Eastern Srednogorie involves initial formation of the calc-alkaline and high-K arc magmatism in the Strandzha and East Balkan regions, followed by roll-back induced intra-arc rifting and

*Corresponding author. Present address: Geological Survey of Norway, Trondheim, Norway / Colorado State University, Fort Collins, CO. Telephone: +1 970 4913816. Fax: +41 446321179. E-mail: georgiev@mail.colostate.edu

the formation of high-K, shoshonitic and ultra-high-K magmatism, including primitive ankaramites in the Yambol–Burgas region.

KEY WORDS: *ankaramites; Eastern Srednogorie arc; geochemistry; primitive magmas; source components*

INTRODUCTION

The European section of subduction-related magmatism in the Alpine–Himalayan orogen formed during the complex subduction of the Western Tethys oceanic lithosphere beneath the European continent. The southeastern part of the European Alpine orogen comprises a distinct belt of Late Cretaceous igneous rocks, variably known as the 'Banat–Srednogorie zone' (Popov, 1981, 1987); 'Banatitic magmatic and metallogenic belt' (Berza *et al.*, 1998), 'Laramian belt' (Cioflica & Vlad, 1973) or 'Carpatho-Balkan segment of the Tethyan Eurasian metallogenic belt' (Janković, 1997; von Quadt *et al.*, 2001). The term Apuseni–Banat–Timok–Srednogorie (ABTS) magmatic and metallogenic belt (Popov, 2002) best represents the geographical extent and geological context of this belt and will be used here.

This Late Cretaceous arc contains a wide compositional range of predominantly calc-alkaline magmatic rocks that host some of Europe's largest Cu and Au deposits. The belt is 30–70 km wide and more than 1000 km in length and can be traced more or less continuously from Romania through Serbia to Bulgaria until it reaches the Black Sea (Fig. 1). It has an L-shaped trend, with a north–south orientation from the Apuseni mountains and Banat region extending further south in eastern Serbia (Ridanj-Krepoljin and Timok regions), and then changing to an east–west orientation in Bulgaria.

The Eastern Srednogorie zone occupies the easternmost parts of the ABTS belt, adjacent to the Black Sea. In contrast to the rest of the ABTS magmatic belt, which is characterized by mostly normal calc-alkaline to shoshonitic and predominantly intermediate magmatism, the Eastern Srednogorie zone exhibits significant geochemical variability and a predominance of primitive mafic to intermediate magmas. The most striking characteristic of the mafic magmas is the range of their compositions covering the entire spectrum of chemical series observed in volcanic arcs: from tholeiitic through calc-alkaline to alkaline (shoshonitic) compositions (Boccaletti *et al.*, 1978; Manetti *et al.*, 1979; Stanisheva-Vassileva, 1980, 1989; Popov, 1981; Stanisheva-Vassileva & Daieva, 1990). The magmatism in Eastern Srednogorie exhibits a specific zonation with more evolved calc-alkaline magmas to the south and north and mafic shoshonitic to ultrapotassic magmas in the centre (Georgiev *et al.*, 2006).

The presence of high-K ankaramites in Eastern Srednogorie (Marchev *et al.*, 2007) may provide a key to understanding the origin of the magmatism in this zone. Ankaramites are mafic lavas with a large proportion of olivine and clinopyroxene phenocrysts. They share some common characteristics with other primitive or parental arc magmas, specifically the presence of olivine phenocrysts with Mg number >90, and coexisting Cr-rich or aluminous spinel (Green *et al.*, 2004). The distinctive chemical features of ankaramites are their high CaO content (up to 19 wt %), and high CaO/Al_2O_3 ratios well above the upper mantle value of 0·8, or higher than the CaO/Al_2O_3 ratio of ~1 in picrites (Green *et al.*, 2004). The main phenocryst phase in the arc ankaramites is high-Mg diopside (Mg number ≤ 94), in addition to olivine and Cr-rich or aluminous spinel. Olivine is Mg-rich ($Fo_{94–84}$) and has a characteristically higher CaO and lower NiO content for a given Mg number, compared with olivines from other primitive rocks (Green *et al.*, 2004). Previously, ankaramitic rocks have been interpreted as a variety of picrite enriched in accumulated clinopyroxene crystals (Gunn *et al.*, 1970; Hughes, 1982); however, recent findings of melt inclusions with ankaramitic compositions (Della Pasqua & Varne, 1997; Schiano *et al.*, 2000; Elburg *et al.*, 2006) provide compelling evidence for the existence of such high-CaO melts. The observed chemical characteristics of the ankaramites cannot be reproduced by melting of lherzolite lithologies under hydrous or anhydrous conditions (Della Pasqua & Varne, 1997; Schiano *et al.*, 2000; Kogiso & Hirschmann, 2001; Schmidt *et al.*, 2004), or by fractionation of olivine from lherzolite-derived melts (Kogiso & Hirschmann, 2001). Instead, nepheline-normative ankaramite formation is attributed to melting of amphibole-bearing clinopyroxene-rich lower crustal or upper mantle cumulates (Schiano *et al.*, 2000; Médard *et al.*, 2006).

In this study we combine field geology with whole-rock major- and trace-element, and Sr and Pb isotope data to constrain the origin and evolution of the magmatism in the Eastern Srednogorie zone. Special attention is given to the most primitive ankaramitic magmas and their relation to the more evolved magmatism. We address the problem of the origin of primitive nepheline normative arc ankaramites by combining our results with melt inclusion and phase mineralogy data for the ankaramites, published in a companion paper (Marchev *et al.*, 2009). Xenoliths of pyroxene-rich cumulates found in a basaltic dike are discussed as a likely source for the ankaramite melts. The combined data provide the first integrated study that supports the mostly experimental-based model for nepheline-normative ankaramite formation by melting of clinopyroxene-rich cumulates (Médard *et al.*, 2004, 2006). Melting of the observed amphibole-bearing clinopyroxenite cumulates is quantitatively consistent with thermodynamic and mass-balance modeling of ankaramite formation. The evolution of the more evolved shoshonitic

Fig. 1. Sketch map of SE Europe showing the location of the Apuseni–Banat–Timok–Srednogorie (ABTS) Late Cretaceous magmatic belt (hatched field). Continuous black line represents the main front of the Alpine–Carpathian–Balkan orogen. The studied Eastern Srednogorie zone occupies the easternmost parts of ABTS belt (grey dashed square). Modified after Ciobanu *et al.* (2002).

rocks from Eastern Srednogorie is explained by fractional crystallization of the primitive ankaramitic magmas concurrent with assimilation of basement rocks. The combined information is incorporated into a geodynamic model explaining the origin and evolution of the magmatism in a key segment of the Tethyan arc.

GEOLOGICAL SETTING AND PREVIOUS GEOCHEMICAL DATA

Several tectonic models have been proposed to explain the formation of the ABTS belt. Older models considered it as an extensional structure that originated in an epicontinental rift environment that formed as a result of post-collisional collapse and related asthenospheric diapirism following Early–Middle Cretaceous deformation (Antonijevic *et al.*, 1974; Popov, 1981, 1987). Since the first plate-tectonic interpretations the formation of the ABTS belt has been linked to the continuous subduction of the Vardar Ocean (a branch of the Tethys Ocean) beneath the Serbo-Macedonian–Rhodope massif (Dewey *et al.*, 1973; Boccaletti *et al.*, 1974; Aiello *et al.*, 1977; Hsü *et al.*, 1977; Dabovski *et al.*, 1991; Janković, 1997; Stampfli & Borel, 2004). New plate-tectonic reconstructions and paleomagnetic data show that the Late Cretaceous subduction front had an east–west orientation and the present-day L shape of the ABTS belt resulted from an ~80° clockwise rotation of the Apuseni Mountains and Banat sectors during the Paleogene–Early Miocene (Pătraşcu *et al.*, 1992, 1994; Csontos, 1995; Neubauer, 2002; Fügenschuh & Schmid, 2005; Schmid *et al.*, 2008).

The distribution of the magmatic rocks and the variation in their major-element geochemistry along the ABTS belt has been reviewed in Popov (1981), Berza *et al.* (1998) and Popov *et al.* (2002). Existing geochronological data from the ABTS belt have been summarized by von Quadt *et al.* (2001), Ciobanu *et al.* (2002), Neubauer (2002) and von Quadt *et al.* (2005); until recently, these consisted mostly of K–Ar whole-rock and mineral data. In the Central Srednogorie transect of the belt high-precision U–Pb zircon (von Quadt *et al.*, 2005; Kouzmanov *et al.*, 2009) and Re–Os ages (Zimmerman *et al.*, 2008) reveal a 14 Myr age progression from north to south, which has been explained by hinge retreat (slab roll-back) leading to

crustal thinning in the arc to back-arc region (von Quadt *et al.*, 2005). The slab roll-back model is consistent with the transtensional structures that host the magmatic products and the observed across-strike age progression in the Central Srednogorie and Timok parts of the belt. Conventional high-precision U–Pb isotope dilution thermal ionization mass spectromtry (ID-TIMS) zircon dating and stratigraphic constraints in the Eastern Srednogorie zone reveal a similar 92 to 78 Ma age span of the magmatic activity (Georgiev, 2008).

The Late Cretaceous magmatic products in the Eastern Srednogorie zone occur within SE Bulgaria within the Strandzha Mountains to the south, the Yambol–Burgas depression in the central part and the Eastern Balkan Mountains to the north (Fig. 2). These areas belong to three tectonic zones that represent the main elements of the Alpine thrust belt in the region: the Sakar–Strandzha tectonic zone, Sredna Gora tectonic zone and East Balkan tectonic zone (Fig. 2, inset).

Strandzha Mountains

The Strandzha Mountains (Fig. 2) are a NE-vergent thrust belt with four major thrust slices (Banks, 1997) extending through NW Turkey and SE Bulgaria. The basement consists of high-grade metamorphic rocks with presumably Precambrian protoliths, intruded by Paleozoic granites, followed by locally preserved Paleozoic greenschist rocks and Permian clastic deposits (Okay *et al.*, 2001; Dabovski *et al.*, 2002). The pre-Cretaceous Mesozoic section consists of two low-grade metamorphosed sedimentary units. The autochthonous unit in the central and northwestern Strandzha Mountains comprises more than 2500 m of Triassic carbonates and shallow to deeper marine Jurassic shales and clastic rocks (Dabovski *et al.*, 2002). The allochthonous unit covers the eastern parts of the Strandzha zone and comprises a Late Triassic deep-marine clastic sedimentary sequence, which was thrust above the carbonate rocks of the autochthonous unit in the Middle Jurassic (Banks, 1997). The main phase of deformation in the Strandzha Mountains occurred after the Middle Jurassic and prior to the Cenomanian (Banks, 1997). During the Early Cretaceous the Strandzha zone was exhumed and Cenomanian shallow-marine sediments were deposited. This Cenomanian cover is rarely preserved because of the strong erosion. The whole section is cut by Late Cretaceous intrusive bodies and extensional dike swarms.

To the west, the Sakar–Strandzha zone is separated from the Central Srednogorie zone by a major transform fault with a NE–SW orientation, which is now sealed by the Neogene–Quaternary deposits of the Thrace depression (Ivanov, 1983). The northern border of the Strandzha Mountains with the Yambol–Burgas depression is marked by a zone of intensive fold and fault deformations with NW–SE orientation (Bončev, 1971).

Yambol–Burgas depression

The Yambol–Burgas depression (Fig. 2) is situated between the Strandzha Mountains to the south and the East Balkan Mountains to the north. It is a low-lying area of outcropping Late Cretaceous mainly marine volcanic and volcaniclastic rocks and several intrusions. Basement rocks are not exposed, nor reached by 3300 m deep drill-holes near the town of Pomorie (Fig. 2); however, geophysical data indicate that they are probably similar to the basement in Strandzha (Georgiev *et al.*, 2001). Sedimentation in the Yambol–Burgas depression commenced at the end of the Early Cretaceous with deposition of alluvial, lake and swamp sediments, overlain by Cenomanian shallow-marine deposits. During the Coniacian–Campanian the geodynamic setting changed significantly and deep-marine flysch sediments, limestones and volcanic tuffs were deposited in the evolving Srednogorie intra-arc trough (Nachev & Dimitrova, 1995b), associated with effusive submarine rocks and intruded by shallow plutons. Post-Campanian compression, folding and uplift terminated the trough and the intra-arc successions were transgressively overlain by Maastrichtian shallow-marine limestones and sandstones. The volcano-sedimentary complex has an estimated total thickness of >6000 m (Stanisheva-Vassileva, 1989), and is subdivided in four major groups as shown in Fig. 2 (Dabovski *et al.*, 2009b): Varshilo (Cenomanian–Turonian–Early Coniacian sediments), and Grudovo, Michurin and Burgas (Coniacian–Campanian volcanic rocks and sediments).

East Balkan Mountains

The East Balkan Mountains are an east–west-trending thrust belt of mainly Paleogene age (Doglioni *et al.*, 1996). Their boundary with the Yambol–Burgas depression to the south is marked by a series of steep normal faults west of the town of Aytos, whereas east of Aytos the rocks from Yambol–Burgas are thrust onto the East Balkan flysch sediments. The Mesozoic basement of the East Balkan region consists of Triassic and Jurassic relatively deep-marine limestones, sandstones and flysch-like sediments exposed in a narrow belt (Dabovski *et al.*, 2002). This Mezocoic basement is overlain by Late Cretaceous and Paleogene clay–carbonate and clastic flysch deposits with a total thickness exceeding 2000–3000 m. Sedimentation started in the Cenomanian with deposition of shallow-marine conglomerates, sandstones, siltstones and shales. During the Turonian the area of the East Balkans was subjected to strong extension and deepening of the basin (Nachev & Dimitrova, 1995a). The Turonian to Maastrichtian limestones and thick flysch deposits are associated in some places with intermediate lavas and pyroclastic rocks. The Late Cretaceous successions are covered by continental to shallow-marine Paleogene and Neogene–Quaternary sediments.

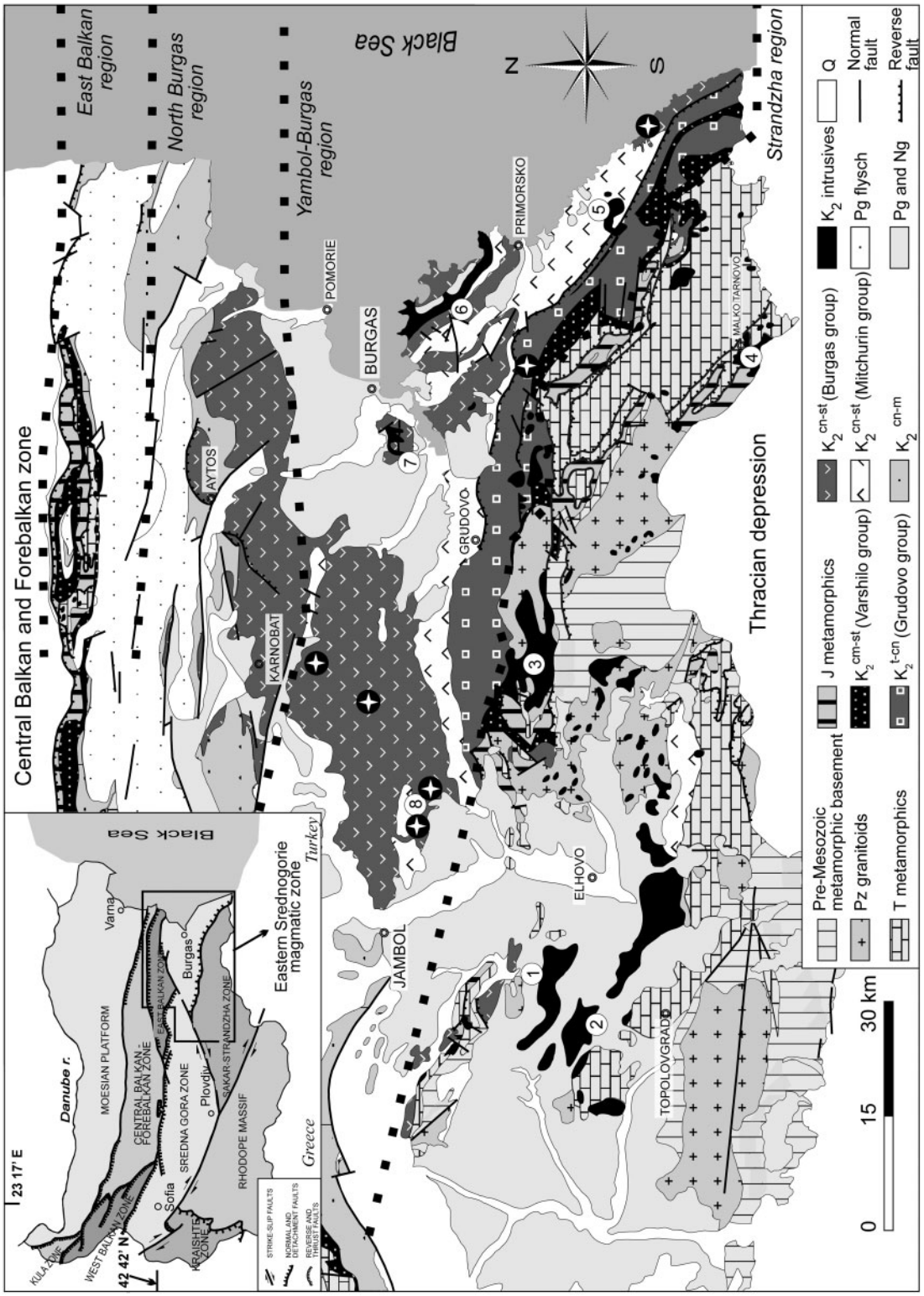

Fig. 2. Geological map of the Eastern Srednogorie magmatic zone, modified after Cheshitev & Kanchev (1989). Bold dotted lines delimit the four magmatic regions in this zone; from south to north these are the Strandzha region, Yambol–Burgas region, North Burgas region and East Balkan region (Dabovski *et al.*, 1991). Circles with stars show the locations of ankaramites. Numbers indicate the most prominent magmatic centers within the Strandzha region (1, Monastery Heights; 2, Granitovo; 3, Oman-Eakya; 4, Malko Tarnovo) and within the Yambol–Burgas region (5, Izgrev; 6, Rossen; 7, Vurli Brjag; 8, Bakadzhicite). Inset: simplified geological map of the tectonic framework of Bulgaria, after Ivanov (1988). The area shown in the main map is outlined. The stratigraphic groups shown in brackets are defined for Yambol-Burgas and North-Burgas regions only.

Subdivision of magmatic regions

The Eastern Srednogorie volcano-intrusive zone (Dabovski, 1991) comprises Late Cretaceous magmatic rocks from all of the three units described above. Based on the local geology and existing whole-rock major-element data, Dabovski *et al.* (1991) distinguished four magmatic regions: the Strandzha volcano-intrusive region, the Yambol–Burgas volcano-intrusive region, the North Burgas volcanic region and the Luda Kamchya volcanic region in the East Balkans. In the current study we use a similar but simplified terminology with the following regions from south to north: Strandzha, Yambol–Burgas, North Burgas and East Balkan (Fig. 2).

The Strandzha region comprises Late Cretaceous multiphase plutons intruded into the pre-Cretaceous basement of the Strandzha Mountains. The largest intrusive bodies are Monastery Heights, Granitovo, Oman-Fakya and Malko Tarnovo (Fig. 2). Dikes are also common, especially in the pre-Mesozoic basement of Strandzha, where they form extensive basic to intermediate dike swarms (Stanisheva-Vassileva *et al.*, 1994). Volcanic rocks are rarely preserved.

The Yambol–Burgas region consists of Late Cretaceous sediments, volcanoclastic deposits, lava flows and pillow lavas. The volcanic structures are of central polyphase, or linear fissure type. The most prominent volcano-intrusive centres are Izgrev, Rossen, Vurli Brjag and Bakadzhik (Fig. 2).

The North Burgas region is a narrow strip of outcropping ultrapotassic ($K_2O/Na_2O > 2$) pillow lavas and pyroclastic rocks, comprising volcanoes of linear fissure type. The subdivision of this zone is based mainly on the elevated K_2O content of the rocks, and there is no clear structural or compositional border with the magmatic products from the Yambol–Burgas region.

The East Balkan region is characterized by minor igneous activity, mostly dikes and subvolcanic bodies intruding Triassic and Jurassic metamorphosed sediments in the Eastern Balkan Mountains. Small remnants of lava flows are also observed.

In contrast to the numerous major-element analyses of magmatic rocks, published trace-element data are limited to 10 basaltic rocks reported by Manetti *et al.* (1979). Those workers argued that the mafic magmas in the Yambol–Burgas region formed by variable degrees of melting of an enriched mantle source (spinel and garnet peridotite), followed by crystal–liquid fractionation of mainly olivine and some pyroxene and spinel. Isotopic studies in Eastern Srednogorie are limited to Sr isotopic data from three intrusions and one volcanic center (Lilov & Stanisheva-Vassileva, 1998; Kamenov *et al.*, 2000).

Previous studies interpreted the Eastern Srednogorie region as an island arc system, consisting of three consecutively formed units: an axial part (Strandzha region), a rear-arc part (Yambol–Burgas region) and the North Burgas back-arc rift (Dabovski *et al.*, 1991; Georgiev *et al.*, 2001). The geodynamic position of the East Balkan region in these models has not been discussed. Recent geochemical studies (Georgiev *et al.*, 2006; Marchev *et al.*, 2009) indicate that magmatism in the intermediate North Burgas and Yambol–Burgas regions is similar and the two units have been merged (see also Ivanov, 1979; Dabovski *et al.*, 2009a). In this study we follow the traditional four-unit subdivision to present additional geochemical and isotope evidence for the similarity between the Yambol–Burgas and the North Burgas regions. The voluminous high-K primitive to intermediate submarine volcanism in these two regions, combined with the deepening of the basin and the orientation of primitive dikes parallel to the arc, suggests that they formed in an extensional setting during the Late Cretaceous. This is in accord with available geophysical data indicating a relatively thin crust (~27 km), observed today below the Yambol–Burgas and North Burgas regions (Yosifov & Pchelarov, 1977). The two units together form the axial part of the Eastern Srednogorie, located between the more evolved and less potassic high-Al basaltic andesites and andesites in the East Balkan region to the north and similar, although more differentiated, volcanic and intrusive rocks in the Strandzha region to the south. Therefore, we interpret this axial zone (Yambol–Burgas and North Burgas regions) as an intra-arc rift, rather than a back-arc rift as previously proposed. Examples of similar intra-arc rifting approximately parallel with the arc are known from the Cascade and Kamchatka arcs (Kersting & Arculus, 1994; Bacon *et al.*, 1997; Conrey *et al.*, 1997).

SAMPLE SELECTION AND ANALYTICAL TECHNIQUES

Ninety-nine magmatic rocks from the Eastern Srednogorie zone were analyzed for major and trace elements in this study. An additional 31 previously published analyses (Boccaletti *et al.*, 1978; Manetti *et al.*, 1979; Marchev *et al.*, 2009) were also used in the discussion. We tried to include in the dataset a broad areal coverage and the full range of compositions of both extrusive and intrusive rocks, and to sample the different stages of the evolution of single volcanic or intrusive centers where field relations indicate clear temporal succession of emplacement. Most abundant are the samples from the Yambol–Burgas region (77), followed by the Strandzha region (21), the North Burgas region (17), and the East Balkan region (9). No estimation of the volume of the Late Cretaceous magmatic rocks in the different regions exists. The tentative volume proportions

based on surface outcrop, stratigraphy and limited geophysical data are 7:10:4:1 for the Strandzha:Yambol–Burgas:North Burgas:East Balkan regions. Five Paleozoic granites from the Strandzha and the Eastern Balkan Mountains and two xenoliths entrained in a mafic dike from the Yambol–Burgas region were also studied. The macroscopically freshest samples were selected for geochemical analysis and petrographic study; all exposed areas and weathered surfaces were carefully removed prior to analysis.

Rocks were powdered in a tungsten-carbide disk vibratory mill. The abundances of the major-element oxides (SiO_2, TiO_2, Al_2O_3, Fe_2O_3*, MnO, MgO, CaO, Na_2O, K_2O, P_2O_5) were determined by X-ray fluorescence (XRF) analysis on $Li_2B_4O_7$-fused glass discs, using a Philips 2404 spectrometer at the University of Salzburg and an Axios PANalytical WD-XRF spectrometer at ETH-Zurich. The reproducibility for the major elements is better than 1% relative. Accuracy and precision were monitored using several international rock standards. Loss on ignition (LOI) was determined by weight difference after heating the powders to 1050°C for 120 min. The bulk-rock major-element composition and selected trace-element abundances in a smaller dataset of rocks were measured by XRF using a Philips PW1480 spectrometer at the University of Florence. MgO, Na_2O and FeO concentrations in these samples were determined by wet chemical analyses.

Trace-element and rare earth element (REE) abundances in most samples were determined on freshly broken cross-sections of the glass discs at ETH Zurich by laser ablation-inductively coupled plasma-mass spectrometry (LA-ICP-MS) using an Excimer 193 nm system with a 60 μm laser beam diameter and 10 Hz repetition rate. The NIST 610 glass was used as an external calibration standard, and the XRF values for Al_2O_3 and CaO were used as internal standards and for cross-checking. The reported concentrations are the average values of three replicate analyses in different domains of the pellet. The analytical reproducibility of the method is concentration dependent and generally better than 5% for concentrations above 1 ppm; and somewhat greater for lower concentrations down to the sub-ppm limits of detection of the method. The accuracy of the method was estimated by repeated analyses of the BHVO and BCR2 USGS standards and was better than 10% for concentrations above 1 ppm and better than 15% for lower concentrations. Nb, Ta and Ni, Pb measured in the BCR2 standard showed higher values of ~20 and 30%, respectively. Experimental setup, limits of detection and a more detailed description of the method have been given by Günther *et al.* (2001). Comparison of the LA-ICP-MS data with solution ICP measurements on selected samples and XRF data for some trace elements shows good agreement between the three methods.

For the isotope analyses, ~100 mg of whole-rock powder was digested in HF and HNO_3, followed by Pb and Sr separation by exchange chromatography techniques on PP columns with Sr spec Eichrom resin. Sr and Pb isotopes were analyzed on a Finnigan MAT 262 by static mode TIMS at ETH Zurich. Sr was loaded with a Ta emitter on Re filaments. The measured $^{87}Sr/^{86}Sr$ ratios were normalized to a $^{88}Sr/^{86}Sr$ value of 8·37521. The mean $^{87}Sr/^{86}Sr$ value of the NBS 987 standard obtained during the period of measurements was 0·710252 ± 12 (2σ, $n = 18$). Pb was loaded with a silica gel on Re filaments. A mass-fractionation correction of 1·1‰ per atomic mass unit was applied, based on replicate analyses of the NBS 982 reference material. Age-corrected Sr and Pb isotope ratios were calculated using Rb, Sr, U, Th and Pb concentrations determined by LA-ICP-MS.

CLASSIFICATION OF ROCK TYPES

Eastern Srednogorie contains a wide range of rock types of variable composition. Intrusive and dike rocks have been classified based on their modal proportions of minerals, and volcanic rocks based on their chemical composition. Sample coordinates and classification are given in Electronic Appendix 1 (available for downloading at http://www.petrology.oxfordjournals.org/).

The rocks from the Strandzha region range from gabbros through diorites to granodiorites and rare granites. Some rocks belong to a monzogabbro–monzodiorite–quartzmonzodiorite–quartzmonzonite–quartzsyenite differentiation trend. The final residues are normally aplites or post-plutonic dikes. Dike swarms are usually basic to intermediate. The magmatic rocks from the East Balkan region are basaltic to andesitic lava flows and subvolcanic porphyry stocks and dikes. In the K_2O vs SiO_2 diagram of Rickwood (1989) the rocks from the Strandzha and East Balkan regions fall mainly in the fields of the tholeiitic, calc-alkaline and high-K calc-alkaline series, whereas in the TAS classification diagram of Le Maitre *et al.* (1989) they range from basalts to dacites (East Balkan) or from basalts to rhyolites (Strandzha).

The magmatic rocks from the Yambol–Burgas and North Burgas regions have been previously classified as picrite, basanite, picro-basalt, absarokite, shoshonite, latite, trachyte and a local variety of ultra-K trachyte named bulgarite (Stanisheva-Vassileva, 1980). In the K_2O vs SiO_2 diagram, the rocks belong predominantly to the shoshonitic series with subordinate high-K calc-alkaline rocks. According to the Le Maitre *et al.* (1989) classification, the rocks range from trachybasalts to trachytes and

subordinate basalts and basaltic andesites. The most mafic rocks (samples SG 11 and SG 12), previously named picrites and basanites, are most probably cumulitic (Marchev *et al.*, 2009). The most mafic non-cumulitic samples of the two regions are characterized by high CaO/Al_2O_3 ratios and have been referred to as ankaramites (Marchev *et al.* 2007, 2009).

PETROGRAPHY

The magmatic rocks from the Strandzha and the East Balkan regions are mostly intrusive rocks and contain hydrous phases, whereas in the central Yambol–Burgas and North Burgas regions they are dominantly basic to intermediate submarine volcanic rocks devoid of hydrous minerals

The basic rock types from the Strandzha region contain plagioclase, amphibole and clinopyroxene ± olivine and Ti-magnetite; orthopyroxene is rare. Several samples from this group, as indicated in Electronic Appendix 2, have a cumulitic origin. The intermediate rocks contain plagioclase, amphibole ± relicts of clinopyroxene ± biotite ± K-feldspar ± quartz. The acid varieties contain variable proportions of quartz, plagioclase and K-feldspar, and minor biotite. The lavas from the East Balkan region are porphyritic with a crystallized groundmass. Their most common phenocrysts are calcic plagioclase, clinopyroxene and green–brown amphibole; plagioclase is the dominant phase in the andesites and clinopyroxene in the basaltic andesites. Amphibole is a major phase in the andesites. Accessory minerals are Ti-magnetite and apatite.

The most voluminous rocks in the Yambol–Burgas and North Burgas regions are of shoshonitic affinity and lack hydrous minerals. Ankaramites and absarokites are strongly porphyritic with fresh clinopyroxene with Mg-rich cores (Mg-number 91–87) and outer zones of Mg-number 85–72 and altered olivine as the only phenocrysts, along with minor spinel inclusions (Cr-number = 75–77) and Ti-magnetite. Abundant plagioclase joins these phases in the basalts and shoshonites, accompanied by phenocrysts of Ti-magnetite and apatite. Groundmasses are fine-grained to glassy, consisting of olivine, clinopyroxene, biotite, plagioclase, K-feldspar, apatite needles and altered glass. The more altered samples contain chlorite, albite, carbonate and zeolites. Regardless of the unsaturated and high-K nature of the rocks, neither leucite nor other feldspathoids have been observed. However, leucite basanites and leucite-bearing basalts (with leucite replaced by a mixture of K-feldspar, nepheline and analcime) have been described in the Bakadzhik center (Stanisheva, 1969; Banushev, 2003). The most evolved trachyandesites, latites and trachytes have plagioclase (often with thin sanidine rims), clinopyroxene and Ti-magnetite set in a perlitic, spherulitic, hyalopilitic or holocrystalline K-feldspar–quartz groundmass. Amphibole and microphenocrysts of orthopyroxene are rarely present in some intermediate lavas (e.g. sample SG2). The less common high-K andesites, described in detail by Boccaletti *et al.* (1978), have abundant plagioclase and hornblende phenocrysts, joined by biotite in the more silicic rocks and augite as phenocrysts and in the groundmass.

The cumulitic sample SG12 consists of equal amounts of olivine ($Fo_{91–85}$) and clinopyroxene (Mg-number 89–69), which make up ~80% of the rock. Melt inclusions in these minerals have ankaramitic compositions similar to the whole-rock ankaramites (Table 1). A more detailed description of the melt inclusions and the mineralogy of the cumulitic rock has been given in a companion paper (Marchev *et al.*, 2009).

Several basaltic dikes from the Izgrev pluton (Fig. 2) carry xenoliths of clinopyroxenite, hornblendite and gabbro, including clinopyroxenite–hornblendite centimetre-scale layered xenoliths up to 10 cm in size. Representative analyses of amphiboles and clinopyroxenes from two xenolith samples (SG 084-5a and SG 084-5b) are given in Table 1. For additional information on the petrography of the rocks from the individual centers in Eastern Srednogorie the reader is referred to Boccaletti *et al.* (1978), Popov *et al.* (1979), Stanisheva-Vassileva (1980) and Dabovski *et al.* (2009*a*). A detailed description of major- and trace-element compositions of phenocrysts from the mafic volcanic rocks of Yambol–Burgas region has been presented by Marchev *et al.* (2009).

GEOCHEMISTRY

Major-element geochemistry

Major- and trace-element data for the studied rocks, xenoliths and melt inclusions from sample SG12 are listed in Electronic Appendix 2. The samples span a wide range in SiO_2 (40–79%), MgO (0·2–25%), FeO_t (1–18%), TiO_2 (0·07–1·40%) and Al_2O_3 (5–25%) contents. However, if we exclude the cumulitic rocks with high contents of MgO and CaO (clinopyroxene accumulation), Al_2O_3 and CaO (plagioclase accumulation) or FeO and TiO_2 (Ti-magnetite accumulation), the variations are much smaller. The most striking characteristic of the magmatic rocks is the systematic north-to-south variation in their alkalinity (Fig. 3) with most of the rocks from the central Yambol–Burgas and North Burgas regions being shoshonitic and nepheline-normative, whereas those from the Strandzha and East Balkan regions belong to the low- to medium-K calc-alkaline series (Fig. 3b) and are subalkaline and Qz-normative (Electronic Appendix 3).

Variation diagrams of major elements vs MgO are shown in Fig. 4. The SiO_2 and Na_2O contents increase systematically with decreasing MgO content, whereas FeO_t and CaO contents decrease with decreasing MgO. The TiO_2 content increases smoothly with decreasing MgO content down to about 3 wt % MgO, indicative of limited

Table 1: Representative analyses of minerals and melt inclusions (MI) from an ankaramitic cumulate (sample SG 12), clinopyroxenite xenolith (sample SG 084-5a) and amphibole-rich xenolith (sample SG 084-5b)

	Ol	MI in Ol	Sp	Cpx	Cpx	Cpx	Cpx	Amph	Amph
Sample:	SG 12	SG 12	SG 12	SG 12	SG 084-5a	SG 084-5b	SG 084-5b	SG 084-5a	SG 084-5b
SiO_2	40·77	49·06	0·08	52·90	53·14	48·91	52·33	43·24	42·33
TiO_2	0·00	0·63	0·60	0·17	0·39	0·92	0·22	1·58	1·47
Al_2O_3	0·04	12·86	8·20	1·76	2·80	5·83	2·22	12·82	13·88
Cr_2O_3	0·04	0·04	41·60	0·52	0·29	0·01	0·25	0·46	0·12
FeO_t	8·92	6·44	34·46	4·95	4·22	5·84	4·38	7·80	9·49
MnO	0·19	0·11	0·30	0·12	0·05	0·24	0·20	0·08	0·10
MgO	49·47	8·00	11·42	16·82	16·74	14·37	16·23	16·84	15·26
CaO	0·46	14·90	0·02	22·59	22·18	23·70	24·10	12·48	12·30
Na_2O	0·01	2·22	0·10	0·16	0·16	0·14	0·07	2·12	1·61
K_2O		2·78				0·05		0·56	1·43
P_2O_5	0·01	0·34			0·01			0·01	0·02
NiO	0·09	0·02			0·01		0·01		
Total	100·0	97·4	96·8	100·0	100·0	100·0	100·0	98·0	98·0
Fo	90·6								
Mg-no.	90·8	68·9	37·1	85·8	87·6	81·4	86·9	79·4	74·1
Fs				7·9	6·8	9·8	7·1		
Wo				45·2	45·4	48·9	48·0		
En				46·9	47·7	41·3	44·9		
CaO/Al_2O_3	10·7	1·2	0·0	12·8	7·9	4·1	10·8	1·0	0·9

Microprobe analyses were conducted at the University of Florence. Olivine (ol) and clinopyroxene (cpx) analyses are recalculated to 100 wt %, and amphibole (amph) to 98 wt % for ease of comparison. The composition of olivine-hosted silicate melt inclusion (MI) is from Marchev *et al.* (2009), who described analytical techniques. All published melt inclusion data are given in Electronic Appendix 2.

Fe–Ti oxide fractionation from the most primitive magmas. In the more evolved samples from the Yambol–Burgas and Strandzha regions, the TiO_2 content decreases with further decrease of MgO, indicating increased fractionation of Fe–Ti oxides. The Al_2O_3 content of the noncumulitic rocks varies from 10 to 20 wt %, increasing smoothly from the most primitive samples to compositions with ~4 wt % MgO. With further fractionation, Al_2O_3 remains constant or decreases slightly. The latter tendency is visible in the rocks from the Strandzha region, and is the result of plagioclase fractionation. The enrichment trend of Al_2O_3 in compositions with MgO more than 4 wt % implies that plagioclase fractionation was insignificant in the early stages of magma evolution, consistent with the observed clinopyroxene-dominated phenocryst assemblage of the most mafic lavas. The Na_2O concentrations in the Strandzha region intrusive rocks increase with decreasing MgO content. A similar but more scattered trend is observed in the other regions. The FeO_t content of the non-cumulitic samples generally decreases with decreasing MgO content.

Trace-element geochemistry

Systematic variations in the XRF and LA-ICP-MS trace-element data with MgO are visible in Fig. 5. The abundance of the incompatible elements such as Rb, Ba and partly of Zr is inversely correlated with the MgO content. The rocks from the Strandzha region have generally lower Rb and Ba concentrations at a given MgO, and show a different trend of Zr enrichment compared with those from the Yambol region, with Zr content being relatively constant in the evolved varieties with MgO <3 wt %. The compatible elements Ni, V and Co (not shown) decrease systematically with decreasing MgO content. Mafic rocks from the Yambol–Burgas region have higher Ni and Co concentrations compared with rocks from the other regions.

Trace-elements patterns of the Eastern Srednogorie magmatic rocks normalized to normal mid-ocean ridge basalt (N-MORB) are presented in Fig. 6. Plotted in the order of increasing compatibility in MORB, any concentration spikes or troughs on the diagram result from processes other than normal, upper mantle decompression

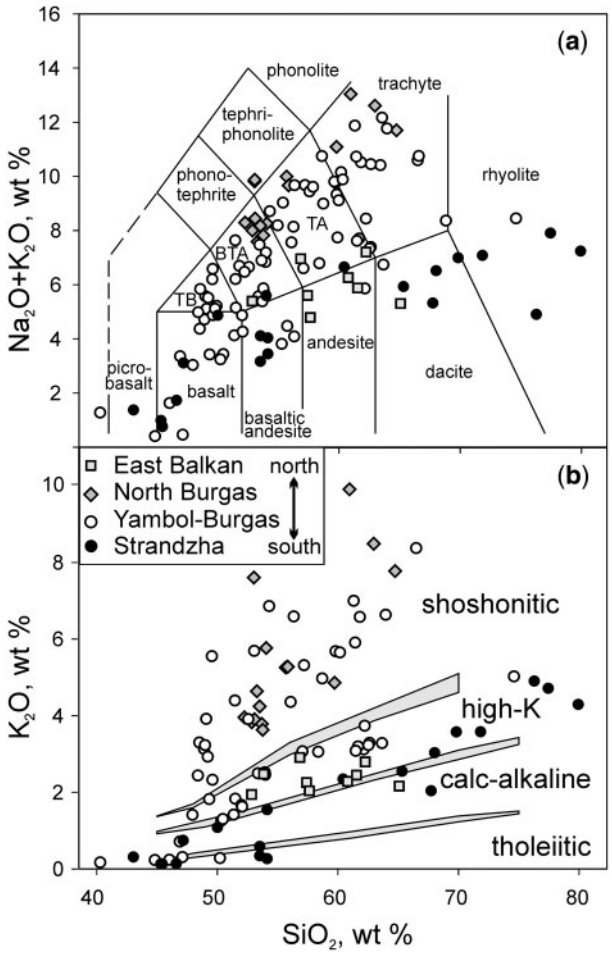

Fig. 3. Chemical classification of rocks from the Eastern Srednogorie zone. (a) Total alkalis vs silica (TAS) diagram, fields from Le Maitre *et al.* (1989); (b) K_2O vs SiO_2 classification diagram (Rickwood, 1989). It should be noted that most of the samples from the southernmost Strandzha region are intrusive rocks.

melting (Sun & McDonough, 1989). The shape of all the patterns in Fig. 6 is typical of magmas formed in subduction-related tectonic settings. The rocks are enriched in large ion lithophile elements (LILE), U, Th and Pb, and to lesser extent in light REE (LREE) relative to the heavy REE (HREE) and high field strength elements (HFSE) (Fig. 6). The HFSE Zr, Hf, Nb, Ta and Ti form distinct negative anomalies in the trace-elements patterns. Only the most evolved varieties do not show Zr and Hf negative troughs. There are large positive K and Pb anomalies, and weaker positive Sr anomalies. In each of the SiO_2 groups, the four regions display remarkably similar patterns, but the relative abundances of the elements, especially the most incompatible ones, are lower in the Strandzha and East Balkan regions compared with the central Yambol–Burgas and North Burgas regions. The rocks from the four regions also have similar chondrite-normalized REE patterns (not shown) with enrichment in LREE and relatively flat HREE patterns typical for rocks from subduction-related geotectonic settings. The most basic rocks have the flattest LREE patterns; with progressive fractionation the LREE enrichment becomes more prominent. The cumulitic intrusive samples display flat REE patterns. The rocks lack significant Eu anomalies; only the evolved acid rocks with $SiO_2 > 58$ wt % show an increasingly negative Eu anomaly. Similar to their higher LILE and HFSE abundances, the majority of rocks from the central Yambol–Burgas and North Burgas regions have higher REE contents compared with rocks with similar SiO_2 contents from the East Balkan and Strandzha regions.

Isotope geochemistry

The measured $^{87}Sr/^{86}Sr$ ratios in the Late Cretaceous igneous rocks display significant variations between 0·70409 and 0·70659 (Table 2). Most samples from the Yambol–Burgas and a few samples from the Strandzha and East Balkan regions have initial Sr ratios between 0·70392 and 0·70437. The published initial $^{87}Sr/^{86}Sr$ data for the Tamarino Bakadzhik volcano (0·7038–0·7045, Lilov & Stanisheva-Vassileva, 1998) and Zidarovo pluton (0·7036–0·7088, Kamenov *et al.*, 2000; Ruskov *et al.*, 2006) in the Yambol–Burgas region show larger variations and partly overlap with our data. The rocks from the Strandzha region have more radiogenic initial $^{87}Sr/^{86}Sr$ ratios compared with the Yambol–Burgas region (Fig. 7a). Initial $^{87}Sr/^{86}Sr$ ratios, calculated from previously published data for the Polski Gradets and Malko Tarnovo plutons in the Strandzha region are similar to our data and are in the range of 0·7048–0·7052 and 0·7044–0·7086, respectively (data from Kamenov *et al.*, 2000). The Late Cretaceous magmatic rocks from the Central Srednogorie zone (Kouzmanov *et al.*, 2009) have consistently higher initial Sr isotopes compared with the studied rocks and overlap only partly with the intrusive rocks from the Strandzha region (Fig. 7a). The Paleozoic basement granites have markedly elevated $^{87}Sr/^{86}Sr$ ratios at 80 Ma ranging from 0·70656 to 0·7092. The least radiogenic compositions (0·70387 and 0·70388) were determined in the clinopyroxenite and hornblendite xenoliths from Izgrev (Table 2).

The $^{206}Pb/^{204}Pb$ ratios of the studied rocks vary between 18·393 and 19·040 (Table 3), and are consistent with the Pb isotopic composition of galenas from ore deposits in Eastern Srednogorie (Amov & Arnaudov, 2000; Kamenov *et al.*, 2000) and K-feldspars from Late Cretaceous intrusions (Kamenov *et al.*, 2000). The variations in $^{207}Pb/^{204}Pb$ are from 15·581 to 15·662, and for $^{208}Pb/^{204}Pb$ from 38·261 to 38·811. The Late Cretaceous rocks form a well-defined positive Pb–Pb isotope correlation, with more radiogenic initial Pb ratios than the common MORB–OIB (ocean

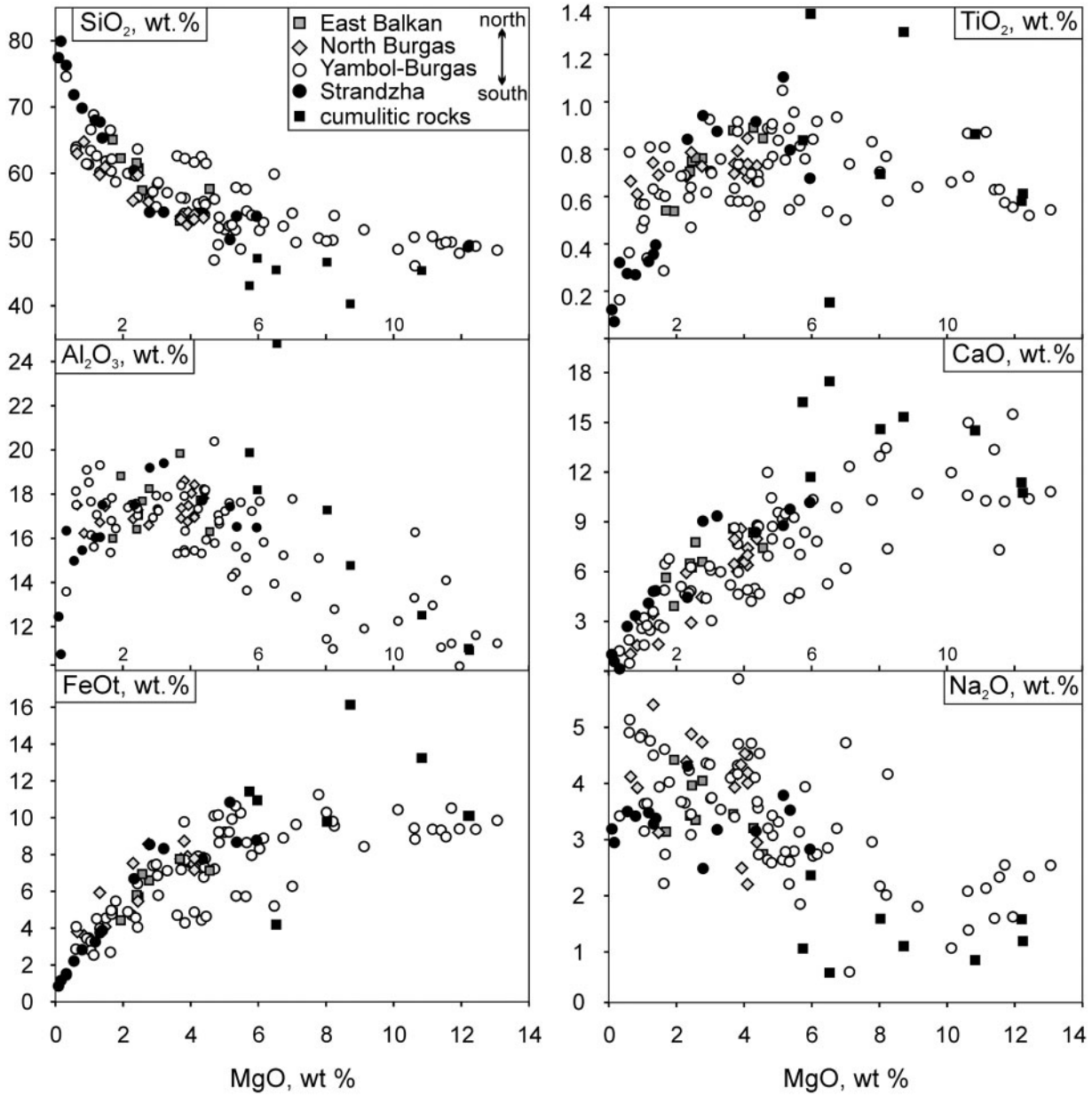

Fig. 4. Variation diagrams for SiO_2, TiO_2, Al_2O_3, CaO, FeO_t, and Na_2O vs MgO (all in wt %). Two cumulate samples SG 11 and SG 12 (MgO ~26 wt %) and the two xenolith analyses (MgO ~15 and 17 wt %) plot outside the area of the diagrams.

island basalt) array (Fig. 7b). The rocks from the adjacent Central Srednogorie zone have a similar range in $^{207}Pb/^{204}Pb$ (Fig. 7b), but extend to lower $^{206}Pb/^{204}Pb$ values. The rocks from the Strandzha region have consistently higher $^{207}Pb/^{204}Pb$ ratios compared with the other regions. The least radiogenic Pb isotopes were measured in the clinopyroxenite and hornblendite xenoliths from Izgrev ($^{206}Pb/^{204}Pb$: 17·920–17·998; $^{207}Pb/^{204}Pb$: 15·575–15·583; $^{208}Pb/^{204}Pb$: 37·620–37·718). The basement Paleozoic granites show clearly elevated Pb isotope ratios (Fig. 7b).

DISCUSSION

Primitive magmas from the Eastern Srednogorie zone

Most mantle-derived subduction-related magmas are affected by complex fractionation and contamination processes that modify their starting compositions (e.g. McCulloch & Gamble, 1991; Hawkesworth *et al.*, 1993; Tatsumi & Eggins, 1995; Elliott, 2003; Tatsumi, 2005). To assess the origin of the magmatism in the Srednogorie segment of the Tethyan arc magmatism, we focused on the

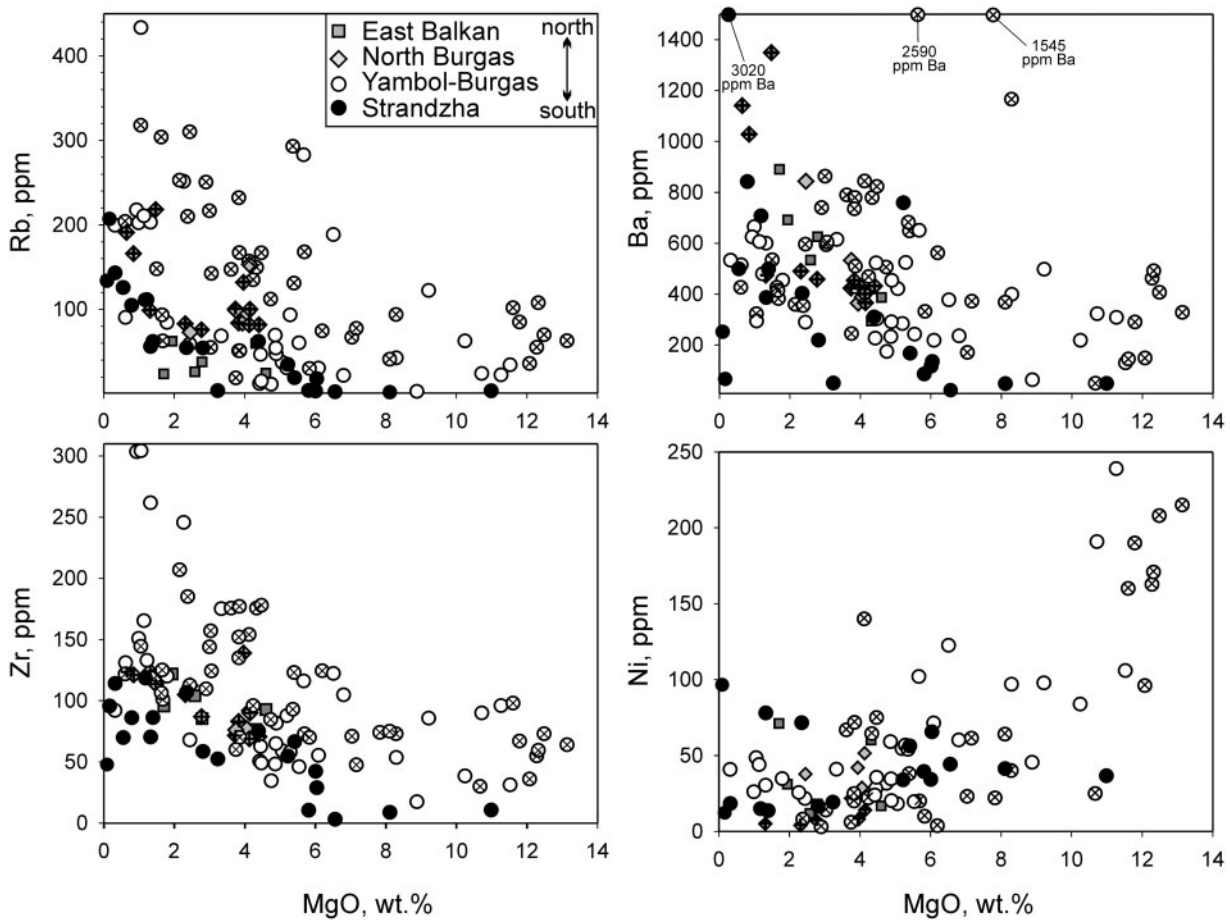

Fig. 5. Variation of Rb, Ba, Zr, and Ni (ppm) vs MgO (wt %) for whole-rock compositions from the Eastern Srednogorie magmatic zone. Symbols with crosses indicate XRF trace-element data; symbols with no crosses indicate LA-ICP-MS data.

most primitive Late Cretaceous rocks within Eastern Srednogorie and filtered the geochemical analyses to select volcanic rocks with relatively elevated MgO contents (>5 wt %) and low SiO_2 (<53 wt %), indicative of limited crystal fractionation. These rocks are also the least affected by crustal assimilation as indicated by their fairly homogeneous initial Sr isotope composition, which is at the least-radiogenic end of the spectrum of all the studied rocks (Fig. 8a). Based on geochemical and mineralogical characteristics, we identify two groups of mafic magmas.

The first group comprises 12 ankaramitic to trachybasaltic lavas from the Yambol–Burgas and North Burgas regions, with MgO >7 wt % and SiO_2 <50·5 wt % with the exception of sample SG102a, which has 51·9 wt % (Electronic Appendix 2; including three analyses from Boccaletti *et al.*, 1978). Most of these lavas have Mg-number > 60, Cr contents ≥350 ppm and Ni contents ≥95 ppm (determined by both XRF and LA-ICP-MS). The most Mg-rich ankaramites have higher Cr contents of ≥550 ppm and Ni contents of ≥160–240 ppm, which makes this compositional group a likely candidate for a near-primary mantle melt. The presence of melt inclusions with similar major- and trace-element composition and high CaO/Al_2O_3 of 1·2 (Fig. 9) provide compelling evidence that the primary magma was very rich in CaO (Marchev *et al.*, 2009).

Using the whole-rock chemistry of the ankaramites presented here, melt inclusion and mineral data, Marchev *et al.* (2009) provided important P–T–fO_2 crystallization constraints for two ankaramites (SG 090 and SG 097) and the cumulate hosting the ankaramitic melt inclusions (sample SG 12). Those workers calculated crystallization temperatures of *c.* 1200–1260°C, at high oxygen fugacities of *c.* ΔFMQ + 2·9 (where FMQ is the fayalite–magnetite–quartz buffer) and ~3 wt % H_2O. These temperatures coincide with the 1220–1260°C typical range of homogenization temperatures of olivine-hosted CaO-rich silica-undersaturated melt inclusions from arc settings worldwide (Della Pasqua & Varne, 1997; Gioncada *et al.*, 1998; Metrich *et al.*, 1999; Schiano *et al.*, 2000). The estimated crystallization pressures of 6–9 kbar (Marchev *et al.*, 2009) correspond to *c.* 20–30 km deep magma chambers;

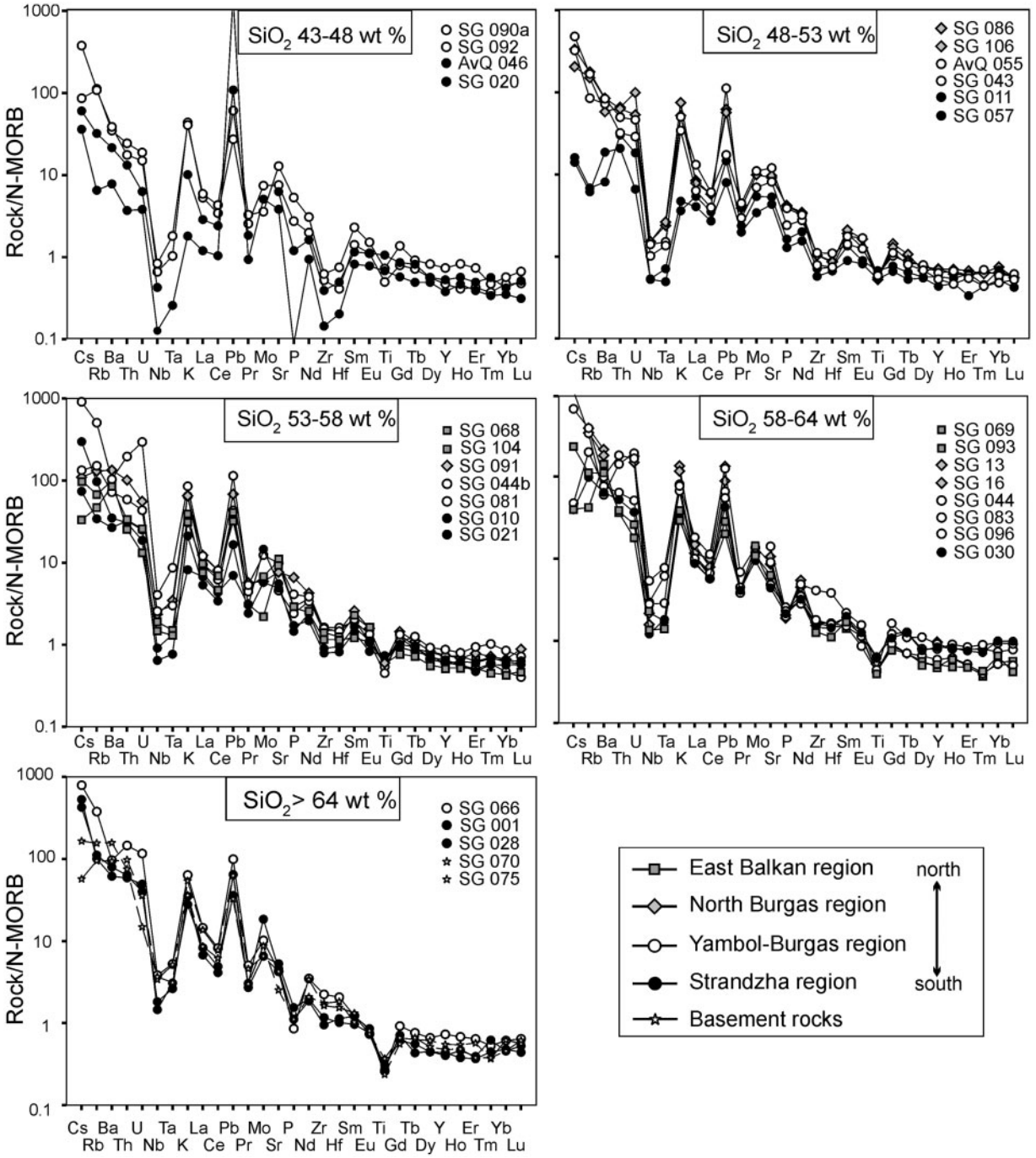

Fig. 6. N-MORB-normalized trace-element patterns of representative samples from the Eastern Srednogorie zone. To avoid the effects of differentiation on the trace-element concentrations, the rocks are divided into five groups based on their SiO_2 content. Within each SiO_2 group, representative samples for each of the four volcano-intrusive regions are reported (sample numbers shown on diagrams). Normalizing values from Sun & McDonough (1989).

this depth is slightly above or near the Moho (27–30 km) in the Eastern Srednogorie zone (Georgiev *et al.*, 2001).

The second compositional group within the Eastern Srednogorie mafic lavas, named here 'other mafic', consists of slightly more evolved mafic lavas with lower CaO/Al_2O_3 ratios. Compared with the ankaramites, six basaltic andesites to basaltic trachyandesites are more SiO_2-rich (51·8–52·3 wt %, sample SG 092 has ~49 wt %) and have lower MgO contents (5·2–6·8 wt %) and lower CaO/Al_2O_3 ratios ranging from 0·66 to 0·49.

Table 2: Sr isotope data for Late Cretaceous igneous rocks, xenoliths and basement rocks from Eastern Srednogorie

Sample no.	Region	Type	$^{87}Sr/^{86}Sr$	2σ	$^{87}Sr/^{86}Sr_{80}$
SG 068	EB	i	0·70489	0·00002	0·70474
SG 093	EB	v	0·70440	0·00001	0·70430
SG 105	EB	v	0·70409	0·00002	0·70400
SG 086	NB	v	0·70456	0·00005	0·70423
SG 087	NB	i	0·70445	0·00020	0·70419
AvQ 053	YB	i	0·70490	0·00002	0·70402
AvQ 054	YB	i	0·70443	0·00001	0·70426
AvQ 057	YB	i	0·70438	0·00000	0·70437
AvQ 058	YB	v	0·70423	0·00002	0·70407
SG 040	YB	i	0·70452	0·00003	0·70429
SG 044	YB	i	0·70643	0·00002	0·70501
SG 090	YB	v	0·70421	0·00002	0·70403
SG 092	YB	v	0·70414	0·00003	0·70397
SG 097	YB	v	0·70420	0·00002	0·70400
SG 099a	YB	d	0·70437	0·00002	0·70414
SG 102a	YB	v	0·70472	0·00001	0·70435
SG 12	YB	v	0·70450	0·00003	0·70392
SG 7	YB	v	0·70450	0·00001	0·70435
AvQ 046	Str	i	0·70438	0·00002	0·70435
AvQ 048	Str	i	0·70659	0·00001	0·70590
AvQ 142	Str	i	0·70419	0·00001	0·70417
SG 001	Str	i	0·70604	0·00004	0·70559
SG 011	Str	i	0·70485	0·00005	0·70482
SG 021	Str	d	0·70523	0·00002	0·70482
SG 028	Str	i	0·70604	0·00001	0·70561
SG 057	Str	i	0·70536	0·00002	0·70533
SG 084-5-a	YB	x	0·70388	0·00004	0·70387
SG 084-5-b	YB	x	0·70393	0·00012	0·70388
SG 070	Bas	i	0·70946	0·00001	0·70870
SG 047	Bas	i	0·70691	0·00003	0·70656
SG 078	Bas?	i	0·71186	0·00004	0·70912

Sr isotope data are corrected for mass-fractionation, 2σ is the absolute standard error of the measurement. The $^{87}Sr/^{86}Sr$ ratio at the time of 80 Ma was calculated using whole-rock Rb and Sr concentrations (Electronic Appendix 2). EB, East Balkan region; NB, North Burgas region; YB, Yambol–Burgas region; Str, Strandzha region; Bas, Paleozoic basement rocks; v, volcanic; i, intrusive; d, dike; x, xenolith.

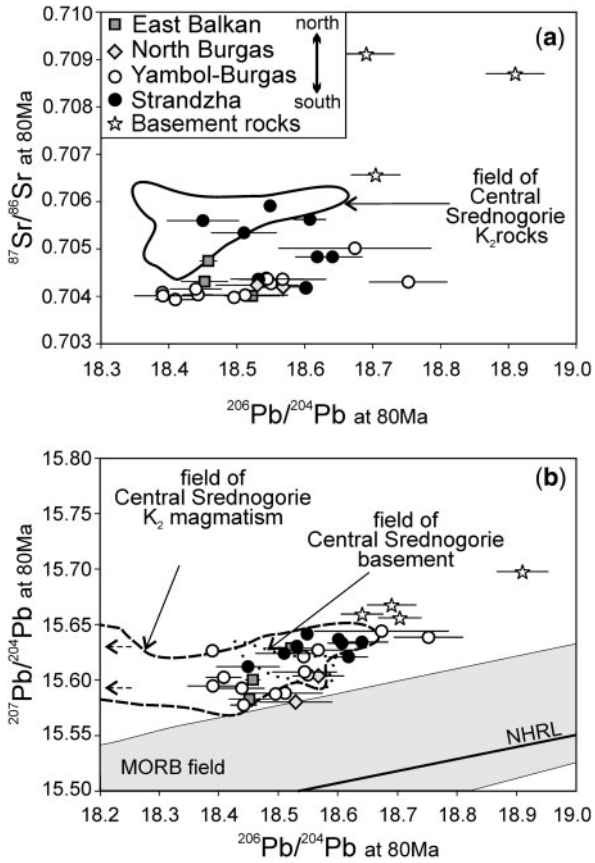

Fig 7. Isotope diagrams for Eastern Srednogorie Cretaceous rocks and Paleozoic basement: (a) $^{87}Sr/^{86}Sr$ and $^{206}Pb/^{204}Pb$; (b) $^{206}Pb/^{204}Pb$ vs $^{207}Pb/^{204}Pb$. Isotope data are age-corrected to 80 Ma. The Northern Hemisphere Reference Line (NHRL; Hart, 1984) is shown for comparison. The field defined by magmatic rocks from the adjacent Central Srednogorie zone is shown for comparison, including the data of von Quadt *et al.* (2005) and Kouzmanov *et al.* (2009) recalculated at 90 and 85 Ma, respectively. The field for MORB is redrawn after Stracke *et al.* (2005). Error bars indicate the error on the age-corrected isotopic ratios, calculated by quadratically adding: (1) the 2σ analytical errors on the TIMS-measured Pb and Sr isotope ratios, which is typically less than symbol size, and (2) errors associated with the propagation of the Pb, U, Th Rb and Sr uncertainties of the LA-ICP-MS measurements on the age-corrected isotope ratios. The small amounts of Rb and ^{235}U in the studied samples result in small age correction-induced errors on the $^{87}Sr/^{86}Sr$ and $^{207}Pb/^{204}Pb$ initial ratios, compared with the errors on the $^{206}Pb/^{204}Pb$ initial ratio.

Unlike the nepheline-normative ankaramites and melt inclusions, these mafic lavas are mostly hypersthene-normative. Their primitive nature is questionable, because they have lower concentrations of Cr and Ni, and could be the products of differentiation of the ankaramites. Two basalts from the Izgrev magmatic center with ~51 wt % SiO_2 and ~11 wt % MgO are also attributed to the 'other mafic' group. They have CaO/Al_2O_3 ratios of ~0·8—transitional values between the ankaramites and the basaltic andesites and basaltic trachyandesites. The compatible trace-element contents of the two rocks (discussed below) indicate that the Izgrev basalts could represent primitive mantle melts.

The chemical composition of the ankaramites, melt inclusions and other mafic rocks is indicated on Fig. 9 and compared with the composition of silica-undersaturated ankaramitic rocks worldwide. The ankaramites have generally lower TiO_2 and Al_2O_3 contents than the rest of the

Table 3: Pb–Pb isotope data for Late Cretaceous igneous rocks, xenoliths and basement rocks from Eastern Srednogorie

Sample no.	Region	Type	$^{206}Pb/^{204}Pb$	2σ	$^{207}Pb/^{204}Pb$	2σ	$^{208}Pb/^{204}Pb$	2σ	$^{206}Pb/^{204}Pb_{80}$	$^{207}Pb/^{204}Pb_{80}$	$^{208}Pb/^{204}Pb_{80}$
SG 068	EB	i	18·496	0·005	15·602	0·004	38·505	0·010	18·457	15·600	38·442
SG 093	EB	v	18·564	0·002	15·588	0·003	38·504	0·008	18·451	15·583	38·315
SG 105	EB	v	18·649	0·012	15·635	0·013	38·498	0·044	18·522	15·629	38·378
SG 086	NB	v	18·728	0·002	15·590	0·001	38·468	0·004	18·529	15·580	38·357
SG 087	NB	i	18·708	0·001	15·611	0·001	38·528	0·002	18·567	15·604	38·451
AvQ 053	YB	i	18·716	0·003	15·598	0·002	38·526	0·005	18·511	15·588	38·408
AvQ 054	YB	i	18·572	0·007	15·606	0·008	38·540	0·022	18·549	15·605	38·519
AvQ 057	YB	i	18·548	0·008	15·622	0·007	38·564	0·019	18·542	15·621	38·563
AvQ 058	YB	v	18·393	0·003	15·627	0·003	38·368	0·010	18·389	15·627	38·364
SG 040	YB	i	18·940	0·003	15·648	0·003	38·692	0·007	18·752	15·639	38·559
SG 044	YB	i	19·040	0·002	15·662	0·002	38·800	0·005	18·673	15·644	38·573
SG 090	YB	v	18·514	0·002	15·581	0·003	38·463	0·010	18·442	15·578	38·384
SG 092	YB	v	18·526	0·002	15·589	0·003	38·261	0·011	18·495	15·587	38·231
SG 097	YB	v	18·525	0·008	15·601	0·007	38·367	0·021	18·390	15·595	38·218
SG 099a	YB	d	18·560	0·008	15·599	0·007	38·497	0·019	18·439	15·593	38·362
SG 102a	YB	v	18·774	0·003	15·637	0·004	38·714	0·011	18·567	15·627	38·539
SG 12	YB	v	18·499	0·010	15·607	0·007	38·438	0·021	18·408	15·602	38·359
SG 7	YB	v	18·716	0·011	15·616	0·008	38·600	0·022	18·544	15·607	38·457
AvQ 046	Str	i	18·531	0·005	15·631	0·005	38·579	0·014	18·531	15·631	38·579
AvQ 048	Str	i	18·576	0·002	15·643	0·003	38·517	0·006	18·548	15·642	38·499
AvQ 142	Str	i	18·628	0·004	15·638	0·003	38·694	0·010	18·601	15·637	38·683
SG 001	Str	i	18·621	0·003	15·620	0·003	38·600	0·009	18·449	15·612	38·429
SG 011	Str	i	18·721	0·004	15·626	0·004	38·809	0·011	18·618	15·621	38·538
SG 021	Str	d	18·782	0·007	15·641	0·006	38·811	0·021	18·640	15·634	38·617
SG 028	Str	i	18·684	0·002	15·637	0·001	38·669	0·005	18·607	15·633	38·566
SG 057	Str	i	18·665	0·003	15·632	0·003	38·748	0·008	18·510	15·624	38·533
SG 084-5-a	YB	x	17·998	0·016	15·583	0·016	37·718	0·045	17·993	15·583	37·715
SG 084-5-b	YB	x	17·920	0·004	15·575	0·004	37·620	0·013	17·915	15·575	37·615
SG 070	Bas	i	19·049	0·006	15·705	0·006	39·310	0·017	18·910	15·698	38·992
SG 047	Bas	i	18·820	0·006	15·662	0·005	38·766	0·015	18·704	15·656	38·570
SG 078	Bas	i	18·822	0·008	15·674	0·007	38·742	0·022	18·690	15·668	38·633
SG 107	Bas	v	18·756	0·002	15·665	0·002	38·945	0·005	18·641	15·660	38·584

Pb isotope data are corrected for mass-fractionation, 2σ is the absolute standard error of the measurement. The Pb–Pb ratios at the time of 80 Ma were calculated using whole-rock U, Th and Pb concentrations (Electronic Appendix 2). Abbreviations as in Table 2.

mafic magmas, and at the same time they are enriched in MgO and CaO (Fig. 9). The K_2O (Fig. 9c) and FeO_t (not shown) variations seem to be independent of the CaO/Al_2O_3 ratio. The melt inclusions have more scattered major-element compositions at a nearly constant CaO/Al_2O_3 ratio of about 1·3. Nevertheless, all other characteristics of the melt inclusions seem to be similar to those of the ankaramitic lavas. Compared with other silica-undersaturated high-calcium arc rocks and melt inclusions, the Eastern Srednogorie ankaramitic compositions have lower TiO_2, Al_2O_3 and CaO and elevated K_2O contents (Fig. 9). Their range in MgO (8–13 wt %) and FeO_t (8–11 wt %) is commonly observed in arc ankaramites. The studied lavas and melt inclusions with the highest CaO/Al_2O_3 (>1·1) range predominantly from 49 to 52 wt % SiO_2 (water-free basis), whereas the reported Si-undersaturated arc ankaramites worldwide reach such high CaO/Al_2O_3 ratios at lower SiO_2 contents (45–49 wt %). Based on the comparison of their major elements, Eastern Srednogorie ankaramites appear to be most similar to the high-Ca inclusions from the Aeolian arc (Metrich & Clocchiatti, 1996; Gioncada *et al.*, 1998) and ankaramitic lavas from Lihir, Papua New Guinea (Kennedy *et al.*, 1990).

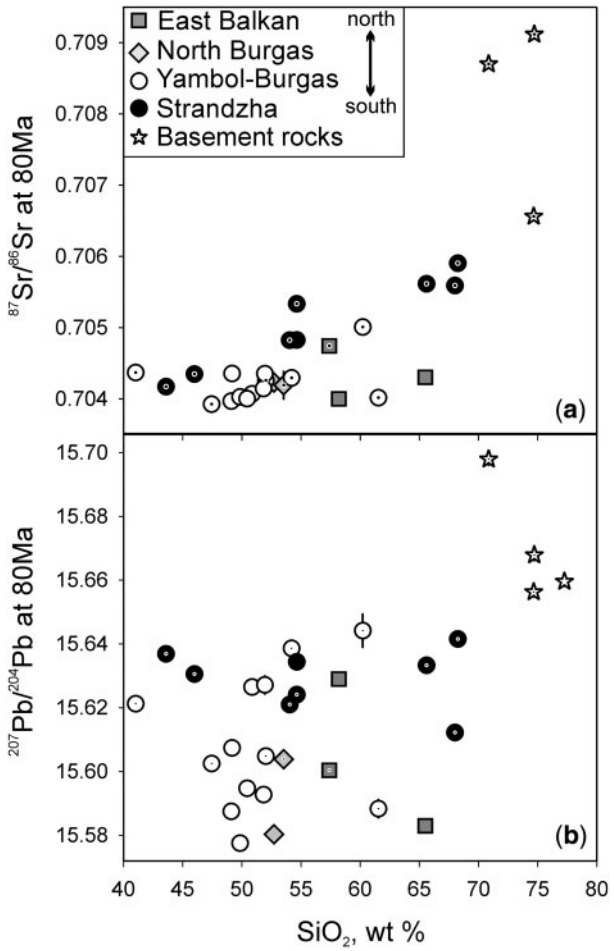

Fig. 8. Variation of $^{87}Sr/^{86}Sr$ and $^{207}Pb/^{204}Pb$ vs SiO_2 (wt %) for the Eastern Srednogorie rocks. Isotope data are age-corrected to 80 Ma. The symbols with dots represent intrusive or cumulitic rocks. Error bar calculation is described in Fig. 7 caption.

The trace-element compositions of ankaramites, other mafic rocks, and melt inclusions in the ankaramites all display very similar patterns on N-MORB-normalized trace-element diagrams, enriched in LILE and relatively depleted in HFSE elements (Fig. 10). All analysed samples show a strong negative Nb trough, and also Zr, Hf and Ti minima. Their chondrite-normalized REE abundances are also similar, enriched in LREE and with relatively flat HREE patterns (Fig. 11). The $(La/Yb)_n$ values of the ankaramitic lavas are ~8, whereas the melt inclusions have lower values of ~5. The absolute abundances of REE are lower in the ankaramites and their melt inclusions, compared with the rest of the mafic magmas.

In summary, nepheline-normative ankaramites with subduction-like trace-element patterns predominate among the least differentiated lavas from Eastern Srednogorie. Non-ankaramitic mafic lavas with elevated MgO content (5–7 wt %) have similar subduction-influenced trace-element patterns, but their lower Cr and Ni contents suggest that they are not primary magmas. Even though some of these lavas seem to form continuous trends with the ankaramites and melt inclusions (Fig. 9b and d), the low-CaO/Al_2O_3, low-K_2O mafic lavas in Fig. 9c show a contrasting trend, suggesting a different genesis.

Origin of Eastern Srednogorie ankaramites

Ankaramites worldwide are divided in two major groups: a silica-rich, alkali-poor hypersthene-normative group and a silica-poor, alkali-rich nepheline-normative group (Schiano *et al.*, 2000; Kogiso & Hirschmann, 2001). The two groups of ankaramitic melts originate from different sources. The genesis of hypersthene-normative ankaramites, found in volcanic arc, back-arc, mid-ocean ridge and oceanic island environments, has been variably explained by: (1) melting of depleted lherzolite (Kogiso & Hirschmann, 2001; Schmidt *et al.*, 2004); (2) melting of CO_2-fluxed lherzolite (Della Pasqua & Varne, 1997; Green *et al.*, 2004); or (3) interaction between a picrite melt and clinopyroxenite (Kamenetsky *et al.*, 1998). These models, however, are not applicable to the formation of high-CaO/Al_2O_3, highly alkaline and silica-undersaturated nepheline-normative rocks such as the studied Eastern Srednogorie ankaramites.

Nepheline-normative ankaramites, found exclusively in arc environments, can be produced by melting of wehrlitic or pyroxenitic lithologies (Schiano *et al.*, 2000; Kogiso & Hirschmann, 2001; Médard *et al.*, 2004). The source can be a wehrlitic mantle (e.g. Barsdell & Berry, 1990), a hydrated sub-arc lithosphere veined by clinopyroxene-rich dikes (Kamenetsky *et al.*, 1998), a clinopyroxene-rich transitional mantle–crust zone similar to that observed in the Oman ophiolite, or wehrlitic lower crustal intrusions that originate from this transitional zone (Benn *et al.*, 1988). On the basis of major- and trace-element chemistry and thermodynamic calculations, Schiano *et al.* (2000) argued that upper mantle or lower crustal pyroxene-rich cumulates within the arc lithosphere are a plausible source of CaO-rich and Si-undersaturated melts. Experimental studies show that nepheline-normative ankaramitic melts become olivine and clinopyroxene saturated at pressures of 0·2–1 GPa and temperatures of 1220–1320°C (Médard *et al.*, 2004).

Amphibole is considered an essential phase in the production of nepheline-normative ankaramites for two reasons. First, its water content significantly lowers the melting temperature of a clinopyroxenite to conditions realistic for arc environments (Schiano *et al.*, 2000; Médard *et al.*, 2004, 2006). Second, melting of amphibole also contributes alkalis and lowers the SiO_2 content compared with pure clinopyroxenite melts and the resulting melts shift towards nepheline-normative compositions.

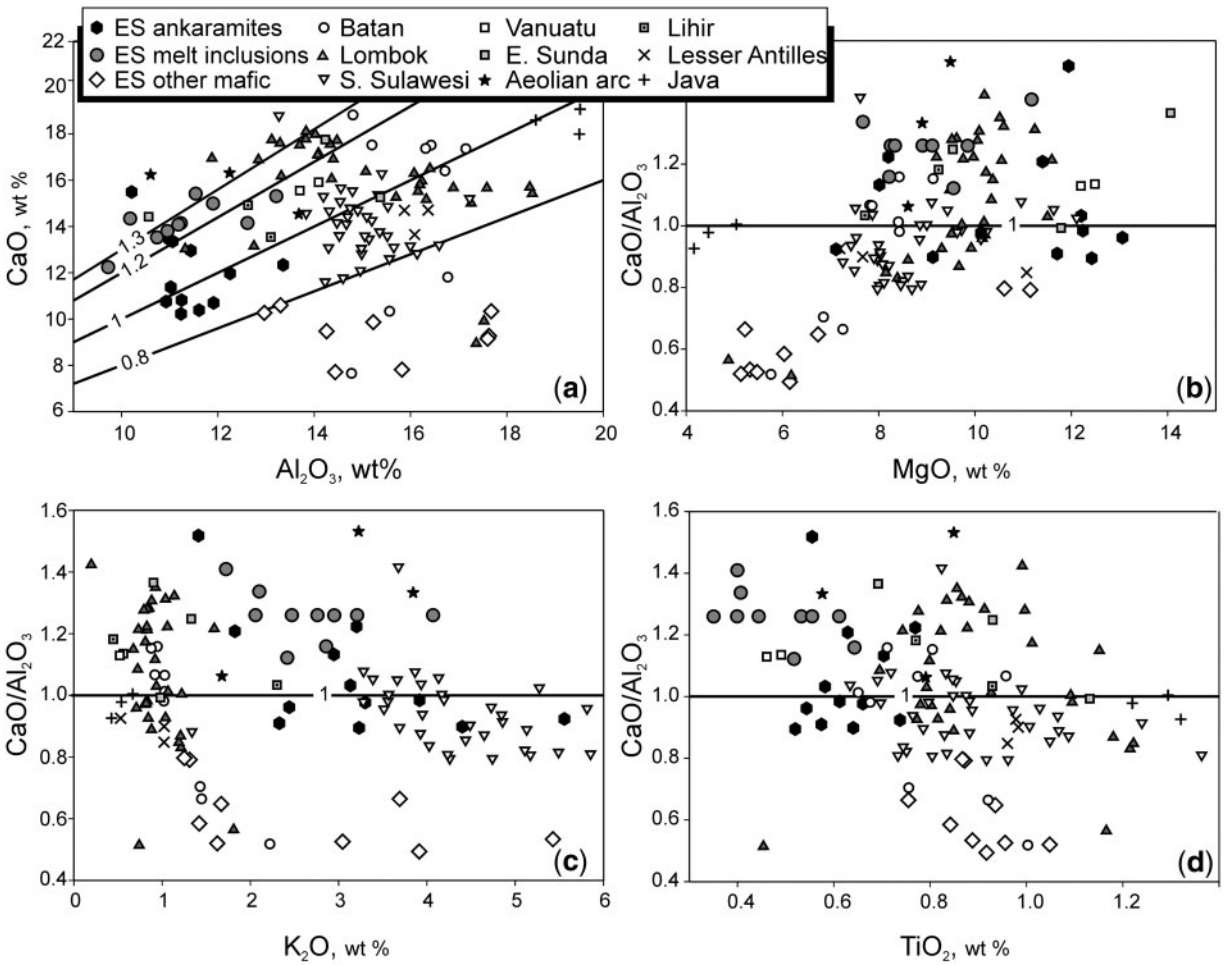

Fig 9. Variation diagrams for Eastern Srednogorie ankaramites and other mafic lavas with MgO > 5 wt %: (a) CaO vs Al_2O_3 (wt %); (b) CaO/Al_2O_3 vs MgO (wt %); (c) CaO/Al_2O_3 vs K_2O (wt %); (d) CaO/Al_2O_3 vs TiO_2 (wt %). Olivine- and clinopyroxene-hosted melt inclusions from the ankaramitic cumulate sample SG 12 (Electronix Appendix 2, data from Marchev *et al.* 2009) are also shown for comparison. Two ankaramitic samples (SG 11 and SG 12), which are not shown on the diagram, with CaO/Al_2O_3 ratios of 1·8 and 2·7 respectively, have high phenocryst proportions, higher MgO and lower Al_2O_3 contents, and have probably accumulated olivine and clinopyroxene phenocrysts. Continuous black lines mark constant CaO/Al_2O_3 ratios. Also shown in the diagram are high-calcium silica-undersaturated melt inclusions with $CaO/Al_2O_3 > 0{\cdot}8$ from South Sulawesi (Elburg *et al.*, 2006), medium-K ankaramitic melt inclusions from Lombok, Indonesia (Elburg *et al.*, 2007), high-calcium melt inclusions from Batan, Philippines (Schiano *et al.*, 2000), and representative analyses of high-calcium silica-

Nepheline-normative ankaramitic melts, similar to those from Eastern Srednogorie, have been experimentally produced by melting of amphibole wehrlite at pressures of 1 GPa and temperatures >1190°C (Médard *et al.*, 2006). The presence of pyroxene, amphibole and layered pyroxene–amphibole cumulate xenoliths in a basaltic dike (sample SG099a) from the Izgrev pluton in the Yambol–Burgas region provides a direct opportunity to test this model of ankaramite genesis. These xenoliths could represent the actual source of the ankaramites, because they are sufficiently rich in clinopyroxene to provide the high CaO, and they also contain amphibole to provide the alkalis for the nepheline-normative character of the ankaramites.

Thermodynamic modeling

To test this link more quantitatively, we calculated the composition of possible partial melts that can be produced from pure clinopyroxenite or mixtures of clinopyroxene with 5 wt % and 15 wt % amphibole cumulate (Table 4), using the Adiabat_1ph program of Smith & Asimow (2005) and its default partition coefficients taken from McKenzie & O'Nions (1991, 1995). Melting models of a depleted MORB mantle composition (Workman & Hart, 2005) are also computed for comparison. The underlying thermodynamic model used for our calculations was pMELTS (Ghiorso *et al.*, 2002) and water was treated as a trace element [details of the method have been given by

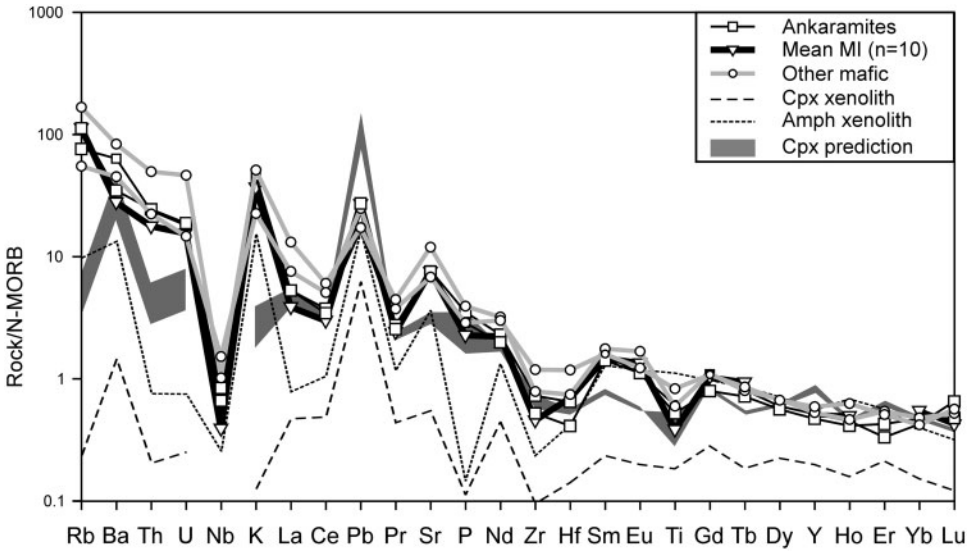

Fig. 10. N-MORB-normalized trace-element patterns of representative ankaramites (SG 097; SG 090a), other mafic lavas from Eastern Srednogorie (SG 043; SG 101), average melt inclusions (MI) from sample SG 12 (Table 4) and the composition of the clinopyroxene- and amphibole-rich xenoliths. The shaded field shows the 1300–1200°C range of predicted model liquids from batch melting of the clinopyroxene xenolith (sample SG 084-5a). Normalizing values are taken from Sun & McDonough (1989).

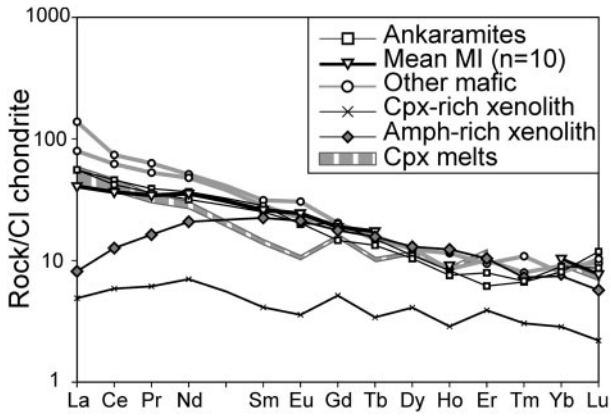

Fig. 11. Chondrite-normalized REE patterns of representative ankaramites (SG 097; SG 090a), other mafic lavas from Eastern Srednogorie (SG 043; SG 101), average melt inclusions from sample SG 12 and the composition of the clinopyroxene- and amphibole-rich xenoliths. The irregular REE pattern of the clinopyroxenite is due to its low concentrations of REE, close to the analytical limit of detection. The shaded field shows the 1300–1200°C range of predicted model liquids from batch melting of the clinopyroxene xenolith (sample SG 084-5a). Normalizing values from Sun & McDonough (1989).

Asimow *et al.* (2004) and Smith & Asimow (2005)]. Calculations were run in an isobaric mode at a pressure of 10 kbar. This pressure was selected based on the following arguments: this is roughly the pressure of the crust–mantle boundary in the region, it exceeds the crystallization pressures of 6–9 kbar calculated for the ankaramites (see above), and amphibole is a stable phase at this pressure. Finally, a considerable amount of the published experimental data on clinopyroxenite melting is at pressures of 10 kbar, which facilitates the comparison of the model with published data. Considering recent calculations for the oxidation state of the melts (Marchev *et al.*, 2009), we used fO_2 buffering at 2 log units above FMQ. Results from the calculations are presented in Electronic Appendix 4 and indicated in Figs 10–13. It should be noted that for compositions AA and CC the model (pMELTS) predicts a clinopyroxene–phlogopite subsolidus assemblage, because hornblende is treated as a K_2O-free phase. In these two models phlogopite melts out at ~4·2% and ~2·5% melting, respectively, followed by clinopyroxene melting.

Results from our modeling confirm that the CaO/Al_2O_3 ratio of the melt is controlled mostly by the abundance of clinopyroxene in the source. For example, melting of a depleted MORB mantle produces a maximum CaO/Al_2O_3 value of only 0·9 at about 23% melting, the point at which clinopyroxene is exhausted (Fig. 12a). Further melting of orthopyroxene + olivine decreases this ratio. The melting fraction is a function of the temperature at a given pressure and therefore the CaO/Al_2O_3 ratio is also dependent on the temperature of melting (Fig. 12b). For a reasonable degree of melting and temperatures higher than 1200°C, a CaO/Al_2O_3 ratio >1 is achieved when clinopyroxene is the dominant component in the source rock (compositions CPX, AA and CC, Table 4). At similar P–T–$x$$H_2O$ conditions, experimental melts from the OCA2 amphibole wehrlite (Médard *et al.*, 2006) reach CaO/Al_2O_3 ratios >1 at higher temperatures and melt fractions (Fig 12), because of the higher starting proportion

Table 4: Starting compositions used for thermodynamic modeling of melting, assimilation and fractional crystallization processes

Composition:	CPX	AMPH	AA	CC	Mean basement	Mean ankaramite	Mean melt inclusions
Ratio CPX:AMPH:	100/0	0/100	85/15	95/5	$n=5$	$n=12$	$n=10$
SiO_2 (%)	52·32	43·00	50·93	51·86	72·41	49·28	50·94
TiO_2 (%)	0·23	1·40	0·41	0·29	0·25	0·63	0·49
Al_2O_3 (%)	2·54	12·20	3·99	3·02	14·19	11·44	11·32
MnO (%)	0·14	0·14	0·14	0·14	0·03	0·17	0·15
MgO (%)	16·85	14·72	16·53	16·74	0·54	10·63	9·00
FeO_t	4·69	9·83	5·46	4·95	1·70	9·77	8·92
CaO (%)	22·40	14·91	21·28	22·03	1·30	11·98	14·20
Na_2O (%)	0·28	1·59	0·48	0·35	3·66	1·76	2·05
K_2O (%)	0·01	1·09	0·17	0·06	3·91	3·14	2·66
P_2O_5 (%)	0·01	0·02	0·01	0·01	0·08	0·37	0·26
CaO/Al_2O_3	8·83	1·22	5·34	7·29	0·09	1·22	1·25
Sc	68	73	69	68	4	31	48
V	133	452	181	149	35	241	202
Cr	1733	508	1550	1672	170	471	889
Ni	170	175	170	170	34	129	128
Rb	0·1	5·3	0·9	0·4	106	69	63
Sr	49	321	90	62	230	842	678
Y	6	15	7	6	16	15	14
Zr	7	17	9	7	123	57	34
Nb	n.a.	0·6	0·1	0·0	7·8	2·1	0·9
Ba	9	82	20	13	631	343	176
La	1·2	1·9	1·3	1·2	27	17	10
Ce	3·6	7·7	4·2	3·8	52	35	22
Pr	0·6	1·5	0·7	0·6	5·2	3·9	3·2
Nd	3·2	9·5	4·2	3·5	19	19	16
Sm	0·6	3·3	1·0	0·7	3·4	4·5	3·9
Eu	0·2	1·2	0·4	0·3	0·6	1·2	1·4
Gd	1·0	3·5	1·4	1·2	2·8	3·5	3·8
Tb	0·1	0·6	0·2	0·1	0·4	0·5	0·6
Dy	1·0	3·2	1·3	1·1	2·9	2·5	n.a.
Ho	0·2	0·7	0·2	0·2	0·5	0·5	0·5
Er	0·6	1·7	0·8	0·7	1·7	1·2	n.a.
Tm	0·1	0·2	0·1	0·1	0·2	0·2	n.a.
Yb	0·5	1·2	0·6	0·5	1·7	1·3	1·7
Lu	0·1	0·1	0·1	0·1	0·3	0·2	0·2
Hf	0·3	0·9	0·4	0·3	3·6	2·0	1·4
Pb	1·8	4·8	2·3	2·0	21	12	8
Th	0·02	0·09	0·03	0·03	14·3	4·5	2·1
U	0·01	0·03	0·02	0·01	2·9	1·8	0·7

Clinopyroxenite xenolith (CPX) and amphibole-rich xenolith (AMPH) were found in a dike in Izgrev pluton in the Yambol–Burgas region (Fig. 2). Compositions AA and CC represent calculated bulk mixtures of the two cumulate xenoliths in the specified proportions.

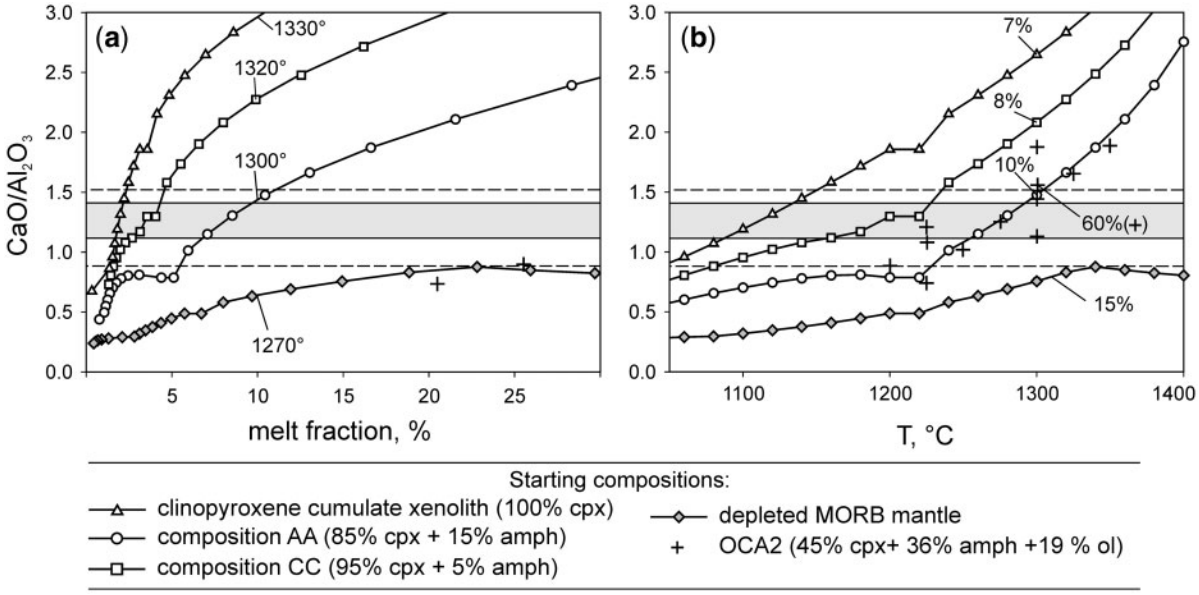

Fig. 12. Relationship between the CaO/Al_2O_3 ratio of the melt and: (a) predicted melt fraction; numbers show the temperature required to achieve 10% melting at the studied conditions; (b) temperature of melting (°C); numbers indicate the melting percentage at 1300°C. Melting process modeled at 1 GPa, $fO_2 = +2$ relative to FMQ buffer and 0·2 wt % H_2O present in the solid assemblage. Also shown is the observed range in the CaO/Al_2O_3 ratios of the studied melt inclusions from sample SG 12 (grey field) and whole-rock ankaramites (dashed lines) from Eastern Srednogorie. The three starting compositions for the melting modeling are given in Table 4. Experimental data on amphibole wehrlite (OCA2) melts at 1 GPa and 1% initial H_2O content after Médard *et al.* (2006). (See text for discussion.)

of amphibole in the source (OCA2 has 36% amphibole, 46% clinopyroxene and 19% olivine). The major-element content of the theoretical melts and the average melt inclusion composition show the best agreement for compositions CPX and CC at temperatures between 1220 and 1300°C, except for the slightly higher TiO_2 and lower K_2O and P_2O_5 content of the predictions. On the CMAS projection (Fig. 13), melting of these compositions reproduces well the ankaramites and melt inclusions from Eastern Srednogorie. The studied ankaramites and melt inclusions plot away from the ol–cpx–opx cotectic line, which excludes a predominant lherzolite source for their formation. Melting of amphibole-free clinopyroxenite results in lower normative nepheline contents, whereas melting of AA composition (85/15 wt % clinopyroxene/amphibole cumulate) shifts the melt compositions towards higher normative nepheline contents than the observed values. These observations are in accord with the published experimental data on olivine-clinopyroxene dominant rocks and amphibole wehrlites, which show that the amount of normative nepheline/hypersthene is a function mainly of the starting composition (Médard *et al.*, 2006). Indeed, the OCA2 amphibole wehrlite experimental melts (36% starting amphibole) have a higher normative nepheline content and plot to the left of the Eastern Srednogorie ankaramites in Fig. 13.

The studied ankaramites and melt inclusions plot in the range of arc-related high-calcium undersaturated compositions, being most similar to lavas from Lihir, Papua New Guinea (Fig. 13). The temperatures and melt fractions, which are necessary to obtain the CaO/Al_2O_3 ratio of about 1·3 in the melt inclusions, increase with the increased proportion of amphibole in the starting material. Experimental studies show that in the pargasite–olivine–clinopyroxene system, amphibole is the first phase that melts: when the temperature is raised to the solidus, amphibole melts incongruently following the reaction amphibole = clinopyroxene + olivine + melt ± spinel (Holloway, 1973; Foden & Green, 1992; Médard *et al.*, 2006). Therefore, resulting melts can substantially increase their CaO/Al_2O_3 ratio only when amphibole is consumed and clinopyroxene enters the melting assemblage. For the pure clinopyroxenite and the CC composition, the calculated temperatures necessary to obtain the CaO/Al_2O_3 ratio of the melt inclusions from Eastern Srednogorie are 1120 and 1220°C, respectively, partly overlapping with the calculated crystallization temperatures of the ankaramites.

Mixing of a clinopyroxenite melt with an even higher CaO/Al_2O_3 ratio (formed at correspondingly higher melting temperature) with a picrite magma of lower CaO/Al_2O_3 provides an alternative scenario for the formation of the Eastern Srednogorie ankaramites. A similar process was proposed for the genesis of ankaramite melt inclusions from Batan, Philippines (Schiano *et al.*, 2000) and is thought to occur in a zone where the magma cools and crystallizes olivine (Schiano, 2003; Médard *et al.*, 2006).

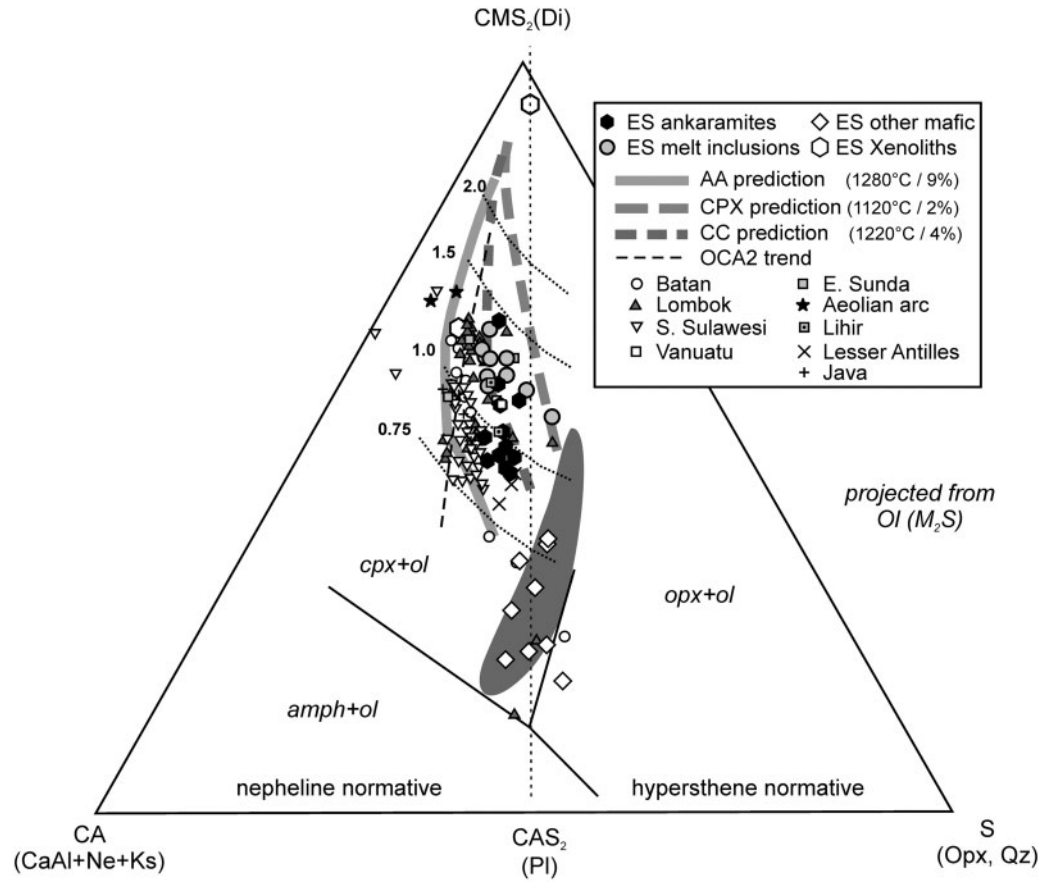

Fig. 13. Schematic CMAS phase diagram showing the Eastern Srednogorie primitive rocks, melt inclusions, xenoliths and predicted isobaric melting trends for three starting compositions at 1 GPa in the 1100–1400°C temperature range. Also shown for comparison are analyses of Si-undersaturated high-calcium melt inclusions and lavas from arc settings worldwide (data sources given in Fig. 9 caption). Data have been recalculated as CMAS components (O'Hara, 1968) using the following formulae: $C = (CaO - 0{\cdot}33P_2O_5 + 2Na_2O + 2K_2O)$; $M = (MgO + FeO^* + MnO)$; $A = (Al_2O_3 + Na_2O + K_2O)$; $S = (SiO_2 - 2Na_2O - 2K_2O)$, and then projected from the olivine (M_2S) onto the Di–Ne–Qz (CMS_2–CA–S) face of the basalt tetrahedron. The continuous black lines for the Ol–Cpx–Amph peritectic, Opx–Cpx–Ol cotectic at 1·2 GPa and water-undersaturated conditions, and Ol–Opx–Amph cotectic at 1·5 GPa at water-saturated conditions are taken from Médard *et al.* (2006, Fig. 8). Grey field delimits the compositions of lherzolite partial melts at 1 GPa, compiled from Médard *et al.* (2006, fig. 9). Starting compositions and xenoliths from Table 4, numbers in parentheses indicate the temperatures and melt fractions necessary to produce CaO/Al_2O_3 ratios of 1·3. Dashed black line is the experimental melt trend of OCA2 amphibole wehrlite (19% Ol, 45% Cpx and 36% Amph) at 1 GPa and 0·5 GPa, taken from Médard *et al.* (2006). Compositions with equivalent CaO/Al_2O_3 ratios (indicated by the numbers) lie on the fine dotted lines.

In Eastern Srednogorie, the presence and nature of this possible picritic component is not clearly defined. Two mafic lavas from the Izgrev center have ~11 wt % MgO (samples AvQ 058 and SG 084a) and plot in the field of lherzolite melts in Fig. 13. They have CaO/Al_2O_3 ratios of about 0·8, which is typical of picrites and at the lower end of the ankaramites. These two rocks have high concentrations of compatible elements (590–710 ppm Cr; 240–290 ppm V; 190–240 ppm Ni), measured by LA-ICP-MS. Taking into account the accuracy and precision of this method for Cr and Ni determinations, these values are at the higher end of the observed range of compatible element concentrations in all the studied lavas, suggesting that the two rocks might represent relatively unfractionated mantle melts.

The lower CaO/Al_2O_3 ratios of these two rocks cannot be formed by fractional crystallization from typical high-CaO magmas, or by lower degrees of melting of the same source material as for the ankaramites. The lower K_2O content of the two basalts (~1·3 wt %) compared with ankaramites with slightly higher CaO/Al_2O_3 ratios (Fig. 9c) and the high Ni and Cr content of the two samples rule out the fractional crystallization hypothesis. The higher Cr and Ni in the two rocks and their notably higher TiO_2 content (~0·9 wt %) compared with the ankaramites (Fig. 9d) are not consistent with derivation of the two lavas by lower degrees of melting of the same starting wehrlite source. Their major- and trace-element features can be best explained either by small degrees of fractional crystallization of an enriched mantle source

melt, or by mixing of a primitive ankaramite melt with a picrite melt having lower K_2O and higher Al_2O_3. The remaining mafic non-ankaramitic rocks plot within or close to the field of experimental lherzolite melts (Fig. 13); they have rather low MgO contents (5·1–6·8 wt %) and lower content of Ni and Cr than typical mantle melts. Their major-element compositions form continuous trends with the ankaramites (Fig. 9b and d), suggesting that at least some of them have been derived by clinopyroxene fractionation from a primitive ankaramitic melt.

Based on these observations, we consider the ankaramites as the one clearly defined primitive melt. However, the lack of primitive lherzolite-derived rocks does not necessarily mean that such melts could not have existed below the crust–mantle boundary. The high density of lherzolite primary melts compared with the overlying crustal rocks, and/or the efficient mixing with the volumetrically dominant clinopyroxenite melts could explain the lack of primitive picritic or boninitic volcanic rocks at the surface.

The chondrite-normalized REE patterns of the calculated clinopyroxenite melts match reasonably well the REE patterns of the ankaramites and the melt inclusions, except for the lower abundances of Sm and Eu (Fig. 11). The higher middle REE in the ankaramites can be explained by melting of small amounts of the studied amphibole cumulate, which has an upward-concave pattern with a maximum at Sm and Eu (Fig. 11). Most of the trace-element concentrations and N-MORB-normalized patterns of the primitive rocks can also be explained by melting of an amphibole-bearing clinopyroxenite. Moreover, the elevated Pb and Ba, as well as the low HFSE and negative Nb, Zr and Ti anomalies in the ankaramite composition compared with N-MORB could also be produced only by melting of a clinopyroxene-rich source (Fig. 10). Thus, melting of a clinopyroxene cumulate at 1 GPa and temperatures of 1200–1300°C is able to explain the trace-element content of the Eastern Srednogorie ankaramites. The presence of residual amphibole (or perhaps) phlogopite in the source may account for the elevated K_2O, Sm and Eu, and partly for Rb in the ankaramites compared with the clinopyroxenite melt prediction. However, the ankaramites and melt inclusions have higher Sr, U and Th contents compared with the predicted melts, which requires addition of those elements from another component.

Subduction modification and sediment addition

The increased abundance of fluid-mobile elements (Rb, Ba, Sr, K, U, Pb) in all of the mafic lavas compared with the predicted wehrlite melts (Fig. 10) could be also linked to the increased fluid flux in a subduction setting. La and Th, however, are normally considered to be immobile in aqueous fluids; they are not enriched during seafloor alteration (Staudigel *et al.*, 1996) or during blueschist- and eclogite-facies metamorphism (Spandler *et al.*, 2003). The most plausible mechanism for their enrichment in arc magmas is addition of sediments or sediment melts to the sub-arc basalt magma source. Plank (2005) showed that variations in Th/La of arc basalts are influenced mostly by the composition and quantity of the subducted sediment component, and are little dependent on the composition of the altered oceanic crust or the mantle. Magmatic fractionation of apatite can also raise significantly the Th/La ratio of the remaining liquid, because apatite favours La 10× over Th (Table 5; Plank, 2005).

The effects of possible sediment addition, apatite fractionation and assimilation of upper or middle crustal granitoids on the wehrlite melt are shown in Fig. 14. In this diagram, mafic lavas from the Yambol–Burgas region and the intrusive rocks from the Strandzha region form two distinct diverging trends. The increase in the Th/La ratios of the Yambol–Burgas lavas is coupled with a slight increase in their initial $^{87}Sr/^{86}Sr$ values from *c.* 0·7040 to 0·7043. This correlation is best reproduced by an assimilation–fractional crystallization (AFC) model involving apatite fractionation and assimilation of Paleozoic granitoids (model A) or sediment (model B), consistent with petrographic evidence for apatite fractionation in the mafic shoshonitic lavas of Eastern Srednogorie (Marchev *et al.*, 2009). Bulk assimilation of sediments (models D and E) or of basement granitoids (model C) can also account for the high Th/La ratios of the ankaramites, but addition of such materials would rapidly shift the Sr isotope composition of the magma towards much higher values than observed. However, the model of bulk assimilation of Paleozoic granitoids by a wehrlite melt (models C and E) approximates the trend defined by the Strandzha region intrusive rocks. Assimilation of other lower crustal granulites or mafic cumulates is also possible but it will not influence significantly the Th/La ratios, because most basaltic cumulates have low Th/La (Plank, 2005).

In summary, interaction of the wehrlite melts with subduction-derived fluids and sediment melts could explain the elevated LILE, Pb, Sr Th and LREE contents of the ankaramites with respect to the predicted cumulate melt compositions (Fig. 10). Addition of such subduction component can explain the observed trace-element concentrations, because it will have high concentrations of both fluid-mobile elements (from slab-released fluids percolating the mantle wedge) and fluid-immobile elements (from sediment melts rising through, and reacting with the sub-arc mantle). This component was probably added to the cumulate melts in the form of a spinel lherzolite-derived melt from the subduction-modified sub-arc mantle wedge.

Isotopic constraints

The isotope compositions of the primitive ankaramites and the remaining mafic lavas are similar and they define a tight cluster (Fig. 15). The two cumulate samples have

Table 5: Mineral–melt partition coefficients used for calculation of the AFC and fractional crystallization models presented in Figs 14 and 16d

	Basaltic rocks* (Fig. 14)		
	Sr	Th	La
Clinopyroxene	0·14	0·00026	0·05
Olivine	0·0035	0·0001	0·0004
Apatite	1·2	7·5	75·00
	Basaltic andesites to andesites† (Fig. 16d)		
	Sr	Rb	Nd
Clinopyroxene	0·054	0·263	0·787
Amphibole	0·172	0·321	1·277
Apatite	2·278	0·370	0·038
Biotite	0·400	3·567	42·083
Plagioclase	0·165	3·324	0·135
K-Feldspar	0·826	3·594	0·032

*Apatite K_d for Th and La from Plank (2005); Th and La K_d values for olivine and clinopyroxene from McKenzie & O'Nions (1991); K_d values for Sr from the GERM database (http://earthref.org/GERM/).
†Mean K_d values for basaltic andesites and andesites from the GERM database.

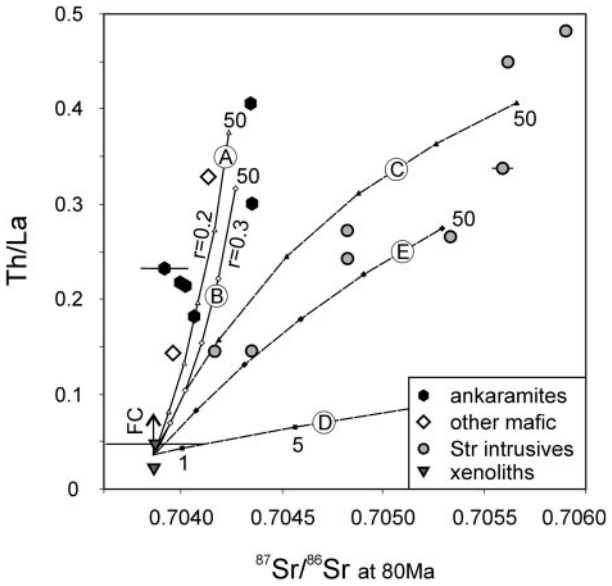

Fig. 14. Th/La vs initial $^{87}Sr/^{86}Sr$ of ankaramites and other mafic rocks from the Yambol–Burgas region and intrusive rocks from the Strandzha region. Starting composition for the modeling is the theoretical CC melt at 1300°C, with 316 ppm Sr, 0·3 ppm Th and 9 ppm La and initial $^{87}Sr/^{86}Sr$ of 0·70386. Two AFC models (equation of DePaolo, 1981) with this starting composition involving fractionation of 1·5% apatite, 80% clinopyroxene and 18·5% olivine reproduce the composition of the ankaramites and other mafic rocks. Model A involves assimilation of basement granitoids (Table 4, initial $^{87}Sr/^{86}Sr = 0·70812$), whereas model B involves assimilation of sediment with the characteristics of the South Sandwich trench sediments (115 ppm Sr, 4·7 ppm Th, 10 ppm La, $^{87}Sr/^{86}Sr = 0·70919$; Plank & Langmuir, 1998). Assimilation of basement granitoids (model C) and the South Sandwich trench sediments (model E) approximate the trend of the intrusive rocks of the Strandzha region, whereas assimilation of GLOSS (327 ppm Sr, 6·9 ppm Th, 29 ppm La, $^{87}Sr/^{86}Sr = 0·7173$; Plank & Langmuir, 1998) results in lower Th/La values at higher $^{87}Sr/^{86}Sr$ (model D). Numbers indicate the per cent of crystallization. Partition coefficients used in the calculations are given in Table 5. Error bars (normally smaller than symbol size) calculated as in Fig. 7.

similar $^{87}Sr/^{86}Sr$ and $^{207}Pb/^{204}Pb$ ratios, but lower initial $^{206}Pb/^{204}Pb$ and $^{208}Pb/^{204}Pb$ compared with the ankaramites (Fig. 15). We argue for two possible explanations of these isotope features. The isotope composition of the assumed wehrlite source is based here on the two studied xenoliths, which are obviously not directly representative of the source with respect to their Pb isotopes. It is possible that the Eastern Srednogorie ankaramites formed by melting of a wehrlite source having similar mineralogy, geochemistry and Sr isotope composition to the studied xenoliths, but slightly more radiogenic Pb isotopes. Alternatively, if we consider the studied xenoliths as the exact source of the ankaramites, then the isotope composition of the cumulate melts must have been modified by interaction with additional components.

Injection of lherzolite-derived melts from the subduction fluid infiltrated mantle wedge at the crust–mantle boundary can trigger melting of the wehrlite cumulates by providing excess heat and fluids. Subsequent mixing of these subduction melts with the wehrlite melts may reproduce the trace-element content and the isotope composition of the ankaramites. However, assimilation of clinopyroxenites by mantle melts, or mixing of lherzolite melts with clinopyroxenite melts, requires a high mixing ratio of at least 40 wt % clinopyroxenite to explain the high CaO/Al_2O_3 ratios of ~1·2 observed in the ankaramites. Moreover, if the lherzolite melts are the dominant component, the resulting mixtures would be too rich in MgO compared with the ankaramites and too rich in Ni to precipitate the low-Ni olivines observed in the cumulitic ankaramite. Therefore we consider the mixing hypothesis possible only if the mixing ratio is in favor of wehrlite melts.

Another possible explanation for this isotopic shift could be the assimilation of other lower crustal lithologies such as cumulate gabbros, granulites or other pyroxene-rich cumulates by the ankaramite magma. LA-ICP-MS and TIMS zircon dating is consistent with this idea and indicates the presence of inherited zircons with an age of 460 Ma in rocks from the Yambol region, even in some primitive ankaramites (Georgiev, 2008). Further speculations on the lithology of the source rock of these 460 Ma zircons, however, require additional age dating and geochemical

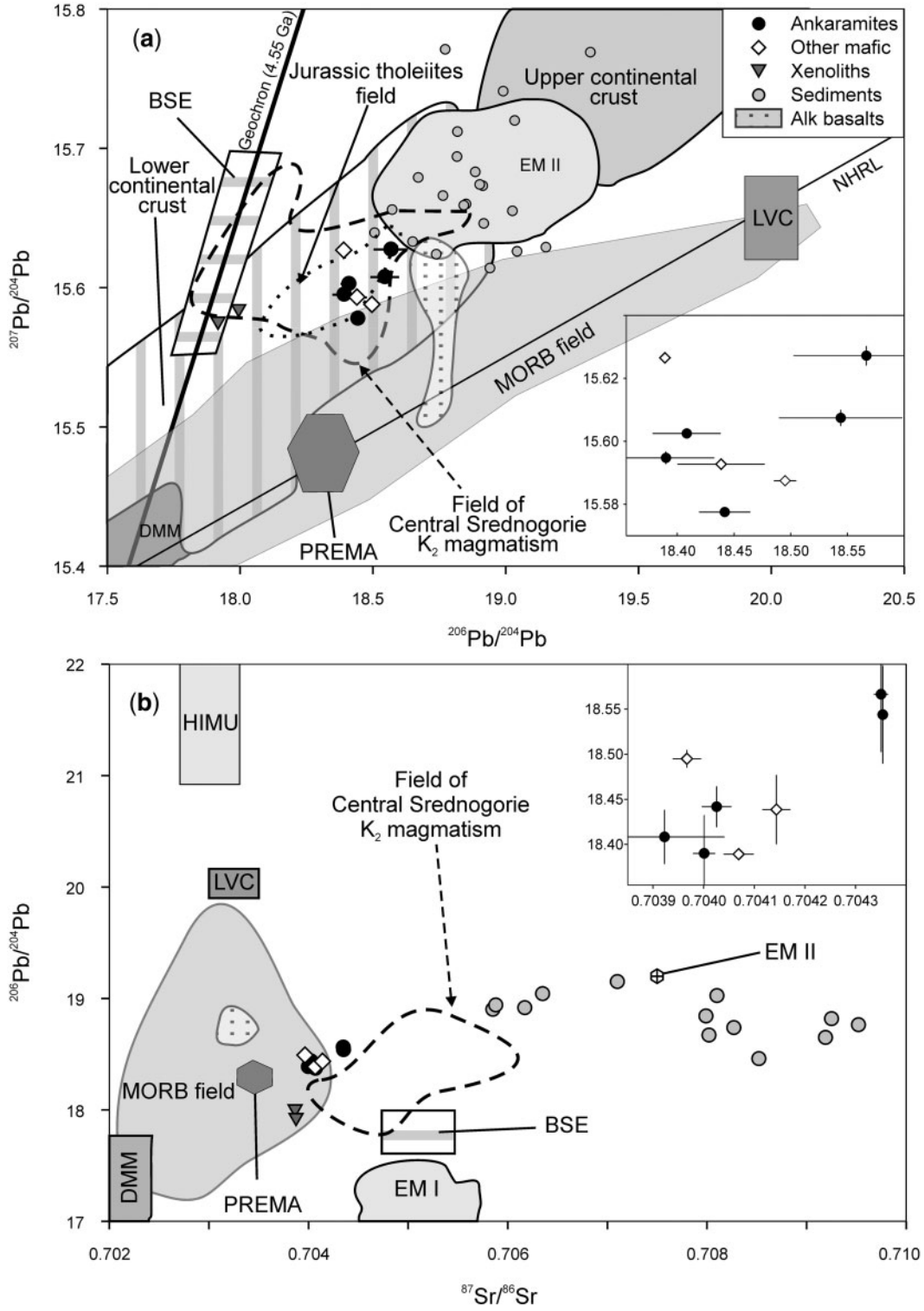

Fig. 15. Isotope diagrams comparing the ankaramites and other mafic lavas from Eastern Srednogorie with the studied xenoliths, currently subducting sediments (compilation from Gasparon & Varne, 1998; Plank & Langmuir, 1998), the Low Velocity Component (LVC) of the European asthenosphere (Hoernle *et al.*, 1995), and younger (~28 Ma) alkali basalts from the Eastern Rhodopes (P. Marchev, unpublished data, age-corrected). MORB field is redrawn after Stracke *et al.* (2005). Fields of depleted MORB mantle (DMM), bulk silicate Earth (BSE), enriched mantle type I (EM I), mantle with high U/Pb ratio (HIMU), frequently observed prevalent mantle composition (PREMA) are taken from Zindler & Hart (1986). The isotopic composition of enriched mantle type II (EM II) is taken from Faure & Mensing (2005). The fields of the lower and upper continental crust are redrawn after Rollinson (1993). (a) $^{206}Pb/^{204}Pb$ vs $^{207}Pb/^{204}Pb$. The field defined by magmatic rocks from the adjacent Central Srednogorie zone is from von Quadt *et al.* (2005) and Kouzmanov *et al.* (2009), recalculated at 90 and 85 Ma, respectively. Also shown here are Jurassic island-arc tholeiites from the Eastern Rhodopes after Bonev & Stampfli (2008), calculated at 180 Ma. (b) $^{87}Sr/^{86}Sr$ vs $^{206}Pb/^{204}Pb$. Isotope data for the Eastern Srednogorie rocks and xenoliths are age-corrected to 80 Ma. The two insets show a close-up view of the Sr and Pb isotope data for the ankaramites and other mafic rocks. Error bar calculation is described in Fig. 7 caption. The Northern Hemisphere Reference Line (NHRL) is taken from Hart (1984).

studies on the various basement lithologies exposed in the Strandzha region.

The isotope composition of the wehrlite melts could be shifted to higher $^{206}Pb/^{204}Pb$ and $^{208}Pb/^{204}Pb$ values by mixing with small amounts of asthenospheric material, or alkali basalts derived predominantly from the asthenosphere (Fig. 15). The asthenosphere below Europe, represented by the Low Velocity Component (LVC; Hoernle *et al.*, 1995), has a more uniform and radiogenic Pb isotope and less radiogenic Sr isotope composition compared with the xenoliths. Addition of such material to the xenolith melts would shift the Pb ratios. Mixing of the wehrlite melts with small amounts of alkali basalt melts, isotopically similar to the the Rhodope Massif alkali basalts (Marchev *et al.*, 1998), would have a similar effect (Fig 15). However, the LVC and the Rhodope alkali basalts have markedly less radiogenic Sr isotope compositions (Fig. 15b) and hence their contribution to the ankaramite magma must have been volumetrically insignificant. Additionally, we find no evidence for significant involvement of such a source in the trace-element chemistry of the most primitive rocks and melt inclusions, which would result in increased Nb and Ta contents and steep HREE chondrite-normalized patterns.

Depth of crystallization of the studied xenoliths

The origin of the studied xenoliths and especially their depth of formation are central for the interpretation of the ankaramite magmatism in Eastern Srednogorie. However, the lack of garnet, Cr-spinel, olivine or orthopyroxene in the cumulates hinders the use of the most commonly applied thermobarometers. The presence of amphibole in the xenoliths indicates a hydrous parental magma and constrains the upper limit of the crystallization temperatures at the limit of amphibole stability to less than 1050–1100°C (Hill & Boettcher, 1970; Holloway & Burnham, 1972; Allen *et al.*, 1975; Jenkins, 1983). Similarly, the maximum crystallization pressure of the cumulates is constrained by the upper limit of amphibole stability to ~2·5 GPa (Hill & Boettcher, 1970; Allen *et al.*, 1975; Mysen & Boettcher, 1975). High-pressure experimental work on primitive basalts and high-Mg andesites clearly demonstrates that olivine-free predominantly pyroxenite ultramafic cumulates at the base of arc sections crystallize from hydrous (>3% H_2O) magmas at pressure of 1·2 GPa (Müntener *et al.*, 2001). The rarity of olivine in the experiments is explained by the narrow crystallization temperature interval of olivine-bearing assemblages in a relatively SiO_2-rich primary melt and/or by olivine consumption by the peritectic reaction olivine + liquid → pyroxene. This study indicates that in the upper mantle or lower crust and under H_2O-undersaturated conditions, crystallization of plagioclase is suppressed. Experimental work on the effect of water on tholeiitic basalt phase equilibria show that at low-pressure conditions of 1 kbar plagioclase starts to crystallize before clinopyroxene at all water contents (Feig *et al.*, 2006). Even at higher pressures of 5 kbar, plagioclase starts to crystallize before clinopyroxene as long as the water content of the melt is less than ~4 wt % (Feig *et al.*, 2006). The lack of plagioclase in the studied xenoliths therefore indicates relatively deeper conditions of crystallization for the clinopyroxenite cumulates. Clinopyroxenes from the xenoliths SG 084-5a have high Mg-number of ~87·6 (Table 1), indicating that the melts that crystallized those pyroxenes were primitive enough to be in equilibrium with mantle olivine, based on a $K_D = 1{\cdot}2$ for Fe–Mg exchange between olivine and clinopyroxene in Mg-rich magmas (Kawasaki & Ito, 1994). The high Mg-number of the clinopyroxenes from the studied xenoliths, combined with their high Cr_2O_3 contents of ~0·3 wt % and low Al_2O_3 contents (<3 wt %) are characteristic for clinopyroxenes from ultramafic and mafic rocks from the base of the arc sections in Alaska (De Bari & Coleman, 1989; De Bari, 1997; Greene *et al.*, 2006), the Aleutians (Conrad & Kay, 1984) and Kohistan (Müntener *et al.*, 2001; Jagoutz *et al.*, 2007). The Al^{VI}/Al^{IV} ratio of clinopyroxenes from SG 084-5a varies between 0·2 and 1·0 and the minerals plot in the granulite–clinopyroxenite field of the Al^{VI} vs Al^{IV} diagram of Aoki & Shiba (1973), outside the field of low-pressure phenocrysts in volcanic rocks. However, the NaO content of the clinopyroxenes (~0·2 wt %) is at the lower end of typical spinel- or garnet-lherzolite clinopyroxenes, suggesting that crystallization conditions were shallower than the upper mantle, or close to the upper mantle–lower crust transition. The geobarometer of Nimis (1995), based on cation distribution between M1 and M2 sites in the clinopyroxene structure, provides additional constraints on the pressure conditions at which the xenoliths were formed. Using mineral data from the clinopyroxenite xenolith, calculations with the Cpxbar program of Nimis & Ulmer (1998) and Nimis (1999) gave a pressure range of 4·5–8·5 kbar for an assumed temperature of 1000°C, and 9·3–13·3 kbar for an assumed temperature of 900°C. Based on their high CaO content the cumulates belong to the crustal pyroxenite field (Schiano *et al.*, 2000, fig. 14). Their Pb and Sr isotope compositions fall in the field of lower crustal materials (Fig. 15a) and preclude crystallization from any of the studied Late Cretaceous magmas. The cumulates are therefore more likely to be the products of an earlier magmatic event. Whole-rock isotope compositions indicate a possible genetic link with Jurassic tholeiites from the neighboring Eastern Rhodopes (Fig. 15a; data from Bonev & Stampfli, 2008), and unpublished trace-element data for clinopyroxenes from the xenoliths indicate that they also formed in a subduction-related environment. Based on the above arguments, we conclude that the studied xenoliths most probably represent lower crustal or upper mantle cumulates, which were formed during a previous, possibly Jurassic,

subduction cycle and were later remelted during the Late Cretaceous event to form the ankaramitic magmas.

Origin of more evolved magmas in the Eastern Srednogorie zone

Although the magmatism in Eastern Srednogorie is unusually mafic in composition, only one clearly primitive magma type is evident. Non-ankaramitic mafic rocks can be derived by the fractionation of clinopyroxene plus a small amount of olivine from the ankaramitic primitive magmas, as suggested by variations in the major- and trace-element compositions of the studied rocks (Figs 4, 5 and 9). To test this hypothesis quantitatively and explain the formation of the wide range of compositions in the Eastern Srednogorie arc, we calculated possible fractional crystallization pathways of the primitive ankaramites using the adiabat_1ph program (Smith & Asimow, 2005). For the starting composition we used the mean value of the ankaramites (Table 4), and ran the calculations in isobaric mode and at an oxygen fugacity of +2 FMQ and temperatures decreasing from 1400 to 800°C. After trial-and-error attempts, the most consistent results were obtained at 8 kbar pressure and 2 wt % initial water content. Resulting liquids for these conditions are indicated in Fig. 16, together with volcanic and dike rocks from all the regions of Eastern Srednogorie, the volcanic-dominated Yambol–Burgas and North Burgas regions being best represented. The simulation predicts crystallization of small amounts of spinel starting at 1330°C, ~4% olivine crystallization between 1280 and 1220°C, major clinopyroxene fractionation from 1250°C, and K-feldspar crystallization starting at 960°C. The onset of olivine and clinopyroxene crystallization overlaps with the range of the calculated crystallization temperature for these phases in the ankaramites (Marchev *et al.*, 2009).

The composition of the predicted liquids is similar to the observed range of SiO_2, MgO and Al_2O_3 contents and CaO/Al_2O_3 ratios of rocks with basaltic and basalt–andesitic SiO_2 content (Fig. 16a and b). The FeO_t, Na_2O, CaO and P_2O_5 contents of the predicted liquids (not shown) are also similar to those of the studied basalts and basaltic andesites. Fractional crystallization from the ankaramitic magma can also explain the high K_2O concentrations in the shoshonitic rocks from the Yambol–Burgas and North Burgas regions. Using a least-squares major-element mass-balance calculation, Marchev *et al.* (2009) demonstrated that the series from ankaramite to absarokites can be obtained through clinopyroxene and olivine fractionation in the ratio 3:1 to 4–6:1. The studied high-K calc-alkaline volcanic rocks, however, deviate significantly from the predicted liquid trend. Their evolution can be modeled by fractional crystallization of a similar clinopyroxene–olivine assemblage at the same P–T conditions using the two low-K_2O (~1·3 wt %) and high-MgO (~11 wt %) Izgrev lavas (Fig. 9c) as the starting composition of the lower-K_2O fractional crystallization trend in Fig. 16c.

For the more evolved compositions with $SiO_2 >$ *c.* 58 wt % the model predicts clinopyroxene and K-feldspar crystallization, which leads to increasing Al_2O_3 contents in the remaining liquids until ~23% Al_2O_3 at ~60% SiO_2. In contrast to the prediction, the Al_2O_3 content of the studied andesitic rocks seems to remain relatively constant at *c.* 16·5–17·5 wt % and decreases further with increasing SiO_2 (Fig. 16b). One possible explanation for the discrepancy between the observed and the predicted trend is that the andesites evolved at shallower depths at mid- or upper-crustal levels, assimilating basement granitoids with low Al_2O_3 and high SiO_2. Fractionation of biotite, observed as a phenocryst phase in the rocks from the Strandzha and East Balkan regions and the high-K rocks from the Yambol–Burgas and North Burgas regions, can also account for the SiO_2 vs Al_2O_3 trend of the evolved lavas. The trace elements Sr, Rb and Nd are sensitive indicators of the effects of possible crystal fractionation. The more evolved rocks have significantly higher Rb/Sr ratios compared with the basalts and most of the basaltic andesites (Fig. 16d). From the observed mineral phases in the Eastern Sredsnogorie rocks, feldspars are the only phase that readily accommodates Sr relative to Rb or Nd (Table 5). Therefore removal of feldspars from a basaltic andesite (SG 25 used as a starting point for the models) is able to raise the Rb/Sr ratio of the resulting melt. Fractionation of clinopyroxene, amphibole or a minor amount of apatite will drive the remaining liquids toward higher Sr/Nd values at relatively constant Rb/Sr ratios, whereas biotite fractionation will lower both Rb/Sr and Sr/Nd (Fig. 16d). However, the major-element characteristics of the evolved magmas, such as increasing SiO_2 coupled with small variations in Al_2O_3, are not consistent with simple feldspar fractionation and indicate possible assimilation of basement granitoids. Figure 16d shows an AFC model involving crystallization of Pl, Kfs, Px and small amounts of apatite and assimilation of basement granitoids ($r = 0{\cdot}4$). This model matches relatively well the Rb/Sr and Sr/Nd systematics of the andesitic and rhyolitic rocks but requires a high amount of basement material to account for the major-element features. The relative proportion of plagioclase and K-feldspar does not influence significantly the AFC calculations, as plagioclase and K-feldspar have similar partition coefficients for Sr, Rb and Nd. The increase of Rb/Sr at relatively constant Ba contents (not shown) is indicative of a high plagioclase to K-feldspar ratio in the fractionating assemblage, consistent with the observed plagioclase-dominated assemblage in the evolved lavas. The proportion of fractionated apatite, however, can change the slope of the AFC model curve significantly (Fig. 16d). The andesitic and rhyolitic compositions can be formed by fractionation of a

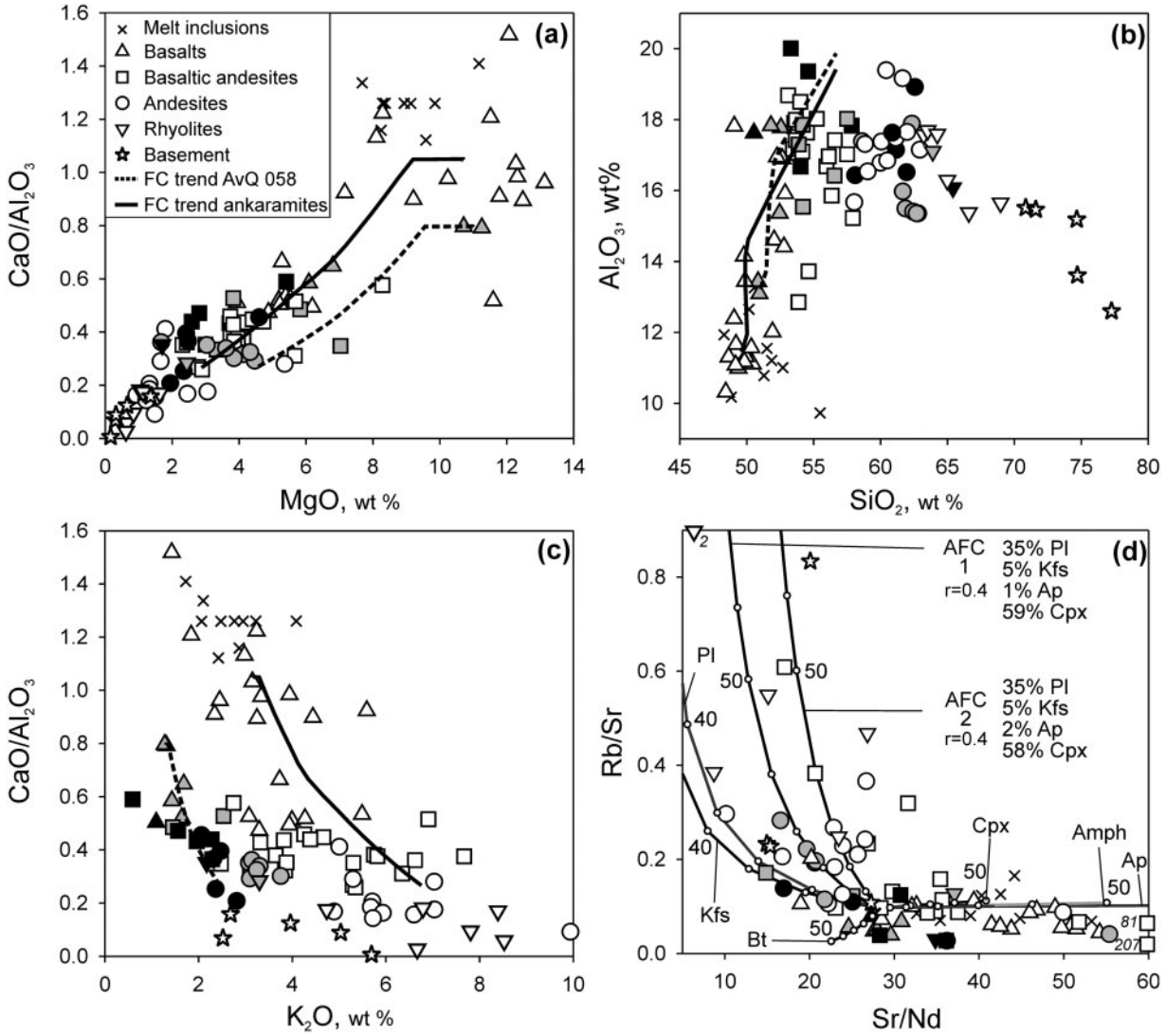

Fig. 16. Variation diagrams for Eastern Srednogorie volcanic rocks: (a) CaO/Al_2O_3 vs MgO (wt %); (b) SiO_2 (wt %) vs Al_2O_3 (wt %); (c) CaO/Al_2O_3 vs K_2O (wt %); (d) Rb/Sr vs Sr/Nd. The rocks are subdivided into four groups based on their SiO_2 content (wt %): basalts (SiO_2 48–53%), basaltic andesites (SiO_2 53–58%), andesites (SiO_2 58–63%) and rhyolites (SiO_2 >63%). Rocks from the Paleozoic basement and the ankaramitic melt inclusions (Electronic Appendix 2) are also shown. Filled symbols are used for high-K rocks from the Yambol–Burgas and North Burgas regions (grey) and calc-alkaline and high-K rocks from the Strandzha and East Balkan regions (black). The bold black line represents the calculated fractional crystallization trend of the average ankaramite magma (from Table 4) at 8 kbar in the temperature range 1350 and 1070°C. With further decrease in temperature the model liquids strongly deviate from the observed compositions (see text for discussion). The dashed black line is a calculation at the same conditions with the basaltic sample AvQ 058 used as a starting composition. Major-element compositions of the rocks and predicted liquids have been normalized to 100% on a water-free basis. (d) represents the effects of fractional crystallization of different minerals on the Rb/Sr vs Sr/Nd of the rocks (FC equation of Neumann *et al.*, 1954). Basaltic andesite SG 25 is used as a starting composition for the models. Two AFC models involving crystallization of plagioclase, clinopyroxene, K-feldspar and apatite can explain the Rb/Sr vs Sr/Nd of the andesitic and rhyolitic compositions. Numbers indicate the percentage of crystallization; partition coefficients used for the calculations are given in Table 5.

plagioclase–apatite-containing assemblage with a 0–3% starting apatite proportion and assimilation of basement granitoids to account for the major-element contents of the rocks.

This model represents a first-order approximation of the assimilation and fractional crystallization process. Further refinement of the AFC model can be achieved by implementing more sensitive indicators of crustal assimilation such as whole-rock Sr and Pb isotope data. Isotope data presented in this study are mostly for the mafic volcanic rocks from the Yambol–Burgas region, which have SiO_2 <53 wt %, and intrusive rocks from the Strandzha region with a wide range of SiO_2 contents and more radiogenic isotope compositions (Fig. 8a and b). The increase

in the initial $^{87}Sr/^{86}Sr$ ratio of the mafic volcanic rocks from ~0·7040 to ~0·7043 (Fig. 15b, inset, and Fig. 17a) is coupled with an increase in the SiO_2 content of the samples from 48 to 52 wt % (Fig. 8a). Although the increase in the Sr and Pb isotope compositions of the mafic magmas can be approximated by assimilation of basement granitoids by the ankaramites (model AB in Fig. 17a), the major- and trace-element compositions of the mafic magmas indicate a minimum amount of granitoid assimilation. Therefore, the variations in the initial $^{87}Sr/^{86}Sr$ of the magmas with $SiO_2 < 53$ wt % can be attributed to a limited amount of sediment addition to the source, or to assimilation of local non-granitoid basement within each of the magmatic centers. Major-element modeling suggests that the more evolved magmas with $SiO_2 > \sim 54$ wt % assimilated significant amount of Paleozoic basement (Fig. 16b and d). Therefore a more likely scenario is the model CB in Fig. 17a, which involves assimilation of basement granitoids by the geochemically most evolved ankaramite (sample SG 102a). The intrusive rocks from the Strandzha region have more radiogenic $^{87}Sr/^{86}Sr$ and $^{207}Pb/^{204}Pb$ initial ratios and plot away from the trend defined by the magmas from the other regions (Figs 7, 8, 14 and 17a). With the exception of one data point, the rocks from the Strandzha region define a mixing line (Fig. 17b). One possible end-member is a magma with a relatively low Sr content (~350 ppm) and $^{87}Sr/^{86}Sr$ (~0·7040), similar to the least radiogenic $^{87}Sr/^{86}Sr$ values of the entire Eastern Srednogorie (point D on Fig. 17b). The other end-member has a higher Sr concentration and more radiogenic $^{87}Sr/^{86}Sr$ ratios of at least 0·7065 (point E in Fig. 17b). Assimilation of Triassic marbles (not analyzed), which are widespread in the Mesozoic basement of the Strandzha region (Fig. 2), would have the desired effect. Pb isotope compositions do not show such clear mixing relations when plotted against 1/Pb (not shown). Further improvements to the AFC model require more detailed information on the chemistry of the phenocryst assemblage in the full range of rock types, a more detailed geochemical investigation of each of the magmatic centers of Eastern Srednogorie, and additional isotope data on the evolved Late Cretaceous rocks and the various basement lithologies.

CONCLUSIONS: ANKARAMITE MAGMATISM IN AN EVOLVING ARC

Based on whole-rock geochemistry, mineral and melt inclusion compositions and Sr–Pb isotope data, we conclude that the primitive ankaramitic magmas in the Eastern Srednogorie zone most probably formed in an intra-arc setting by remelting of a clinopyroxene-rich lower crustal or upper mantle source. Thermodynamic models using clinopyroxene- and amphibole-rich xenoliths as starting compositions are quantitatively consistent with a lower crustal cumulate melting model. Magma genesis is intimately connected with the geodynamic evolution of the Eastern Srednogorie arc and has important implications for plate interaction during Tethys closure in SE Europe. The following two-stage geodynamic model explains the compositional distribution of diverse magma types in the Eastern Srednogorie zone and the characteristic formation of primitive ankaramitic magmas found exclusively in the central parts of the evolving arc system.

The first phase of arc evolution followed the northward thrusting of the Strandzha block and its accretion against the European margin during the Early Cretaceous (Banks, 1997). In the Late Cretaceous, this collision initiated north-dipping subduction of the Vardar Ocean beneath the Strandzha and the East Balkan zone, which at this stage were immediately adjacent to each other. The trench was located south of the present Strandzha–Rhodope Mountains, now covered by young sediments of the Mediterranean basin or possibly the thick Eocene sediments of the Thrace depression. The mantle wedge of the European plate above the subduction zone was infiltrated by fluids ascending from hydrated peridotite dragged downward by the Vardar slab. The fluids migrated upwards and accumulated in a first melt-producing region in the spinel stability field of the lithospheric mantle (Fig. 18a), which initially had the chemical characteristics of MORB source mantle, but became enriched by addition of subducted sediment melts and fluid-mobile elements from the subducted slab, and possibly a small component of asthenosphere-derived melts enriched in radiogenic Pb. These mantle-derived melts rose to the base of the crust, which was thickened by the preceding accretion. Partial crystallization of the magma and assimilation of ~300 Ma Variscan granitoids (Georgiev, 2008) and/or other crustal lithologies led to the emplacement of tholeiitic to calc-alkaline magmas into the middle and upper crust now exposed in the Strandzha and East Balkan regions. This first phase of magmatism occurred in a compression-dominated environment (Fig. 18a), in the period of 90–81 Myr (Georgiev, 2008).

In the second phase of arc evolution, the geodynamic regime evolved to more extensional conditions, as a result of sinking and roll-back of the subducting slab. Evidence for slab roll-back comes from a progressive younging of magma emplacement from north to south, already indicated during the 90–80 Myr period in the Eastern Srednogorie region (Georgiev, 2008) but shown more clearly in the Central Srednogorie (von Quadt *et al.*, 2005). Extension resulting from slab roll-back pulled the East Balkan and the Strandzha blocks apart, thereby opening the Yambol–Burgas and North Burgas regions to subsidence, submarine volcanism and deep-water

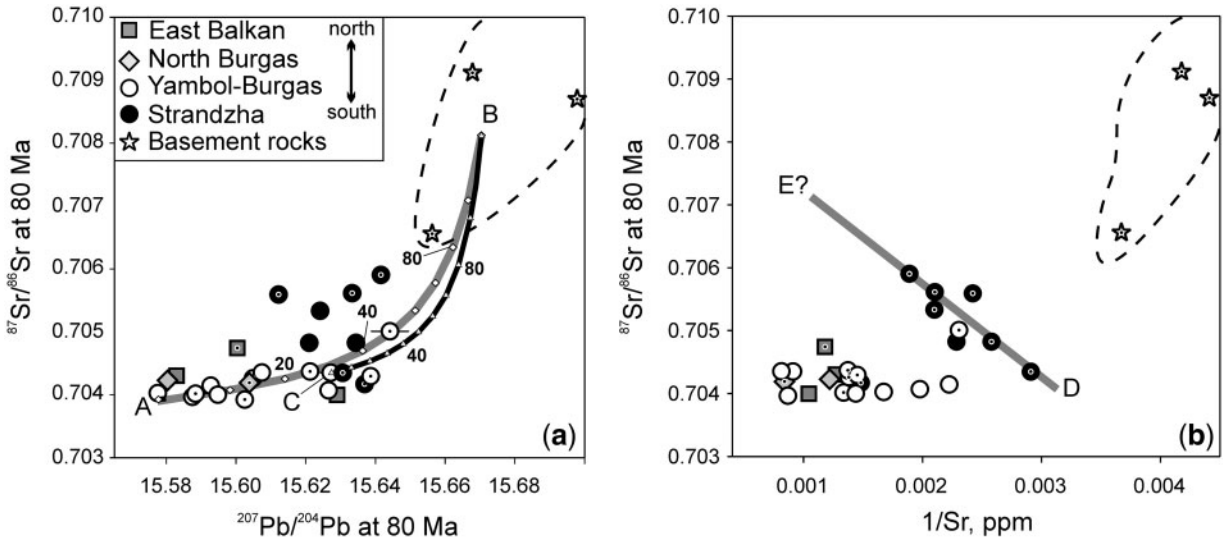

Fig. 17. Isotope diagrams comparing the Late Cretaceous magmatic rocks from Eastern Srednogorie with the local basement, represented by Paleozoic granitoids. Symbols with dots are intrusive or cumulitic rocks. (a) $^{87}Sr/^{86}Sr$ vs $^{206}Pb/^{204}Pb$. Calculated mixing line between (A) the average melt inclusion composition and (B) average basement (from Table 4), as well as sample SG 102a (point C) and average basement (B) are shown. The isotopic values used for the calculation are as follows: for melt inclusions $^{87}Sr/^{86}Sr = 0{\cdot}70392$ and $^{207}Pb/^{204}Pb = 15{\cdot}592$; for the basement rocks $^{87}Sr/^{86}Sr = 0{\cdot}70812$ and $^{207}Pb/^{204}Pb = 15{\cdot}670$. Numbers indicate the percentage of assimilated basement. (b) $^{87}Sr/^{86}Sr$ vs 1/Sr. The grey line is a possible mixing line between two components with different isotope ratios and different Sr concentrations (E and D) (see text for discussion). Dashed line delimits the field of the Paleozoic granitoids. Isotope data are age-corrected to 80 Ma. Error bars (normally smaller than symbol size) calculated as in Fig. 7 caption.

sedimentation. Crustal thinning combined with increased asthenospheric corner flow below the extending crust (Fig. 18b) allowed high-Mg melts to rise from the sub-arc mantle and reach the crust–mantle boundary, which became heated to temperatures at which amphibole-containing clinopyroxenite cumulates started to melt extensively and produced a primitive ankaramitic magma component. The high-Mg island-arc basalts have typical temperatures of 1180–1330°C (e.g. Pichavant *et al.*, 2002), which considerably exceed the breakdown temperature of amphibole (1050°C at 1 GPa; Holloway, 1973), hence underplating of high-Mg basalts into the base of lower crustal clinopyroxene + amphibole ± olivine cumulates is a plausible driver for melting of the cumulates and production of nepheline-normative ankaramites. The presence of amphibole in the source cumulates provided additional alkalis to generate the nepheline-normative character of the ankaramites, as well as additional water facilitating the melting and assimilation process. The studied ankaramites formed by melting of lower crustal cumulates with slightly more radiogenic Pb isotope compositions and similar major- and trace-element compositions to the two studied xenoliths. Alternatively, chemical interaction between partial melts of the studied wehrlite xenoliths and a small amount of subduction-modified mantle melt or subduction fluid can explain the slightly modified Pb isotope composition of the ankaramites, compared with the source cumulates. Crystallization of the ankaramitic rocks from these hybrid parental melts started upon cooling by a few tens of degrees (down to ~1240°C) at pressures close to the crust–mantle boundary (~8 kbar), high water contents and oxidizing conditions. The extensional environment provides the pathways which facilitate rapid ascent and extrusive emplacement of the ankaramitic magmas into a topographically depressed, partly submarine surface environment. Fractional crystallization of the ankaramitic melt in deep-seated magma chambers close to the crust–mantle boundary and assimilation of lower crustal wall-rocks containing predominantly Ordovician zircons (Georgiev, 2008) resulted in the formation of the voluminous mafic shoshonitic volcanism in the central Yambol–Burgas and North Burgas regions of Eastern Srednogorie. The less common high-K calc-alkaline series in these intermediate regions also formed by fractionation of a clinopyroxene–olivine-dominated assemblage, but from a less K_2O-rich starting composition, possibly a fractionated lherzolite melt. Assimilation was limited in the mafic shoshonitic rocks, whereas the andesitic and more evolved rocks in those two regions formed in shallower magma chambers with more significant assimilation of upper crustal lithologies.

This high-K to ultrapotassic, but rather mafic magmatism formed in a narrow time interval between 81 and 78 Ma (Georgiev, 2008). The presence of contemporaneous (81–78 Ma) tholeiitic, calc-alkaline and high-K intrusions in the Strandzha region suggests that wehrlite melts were

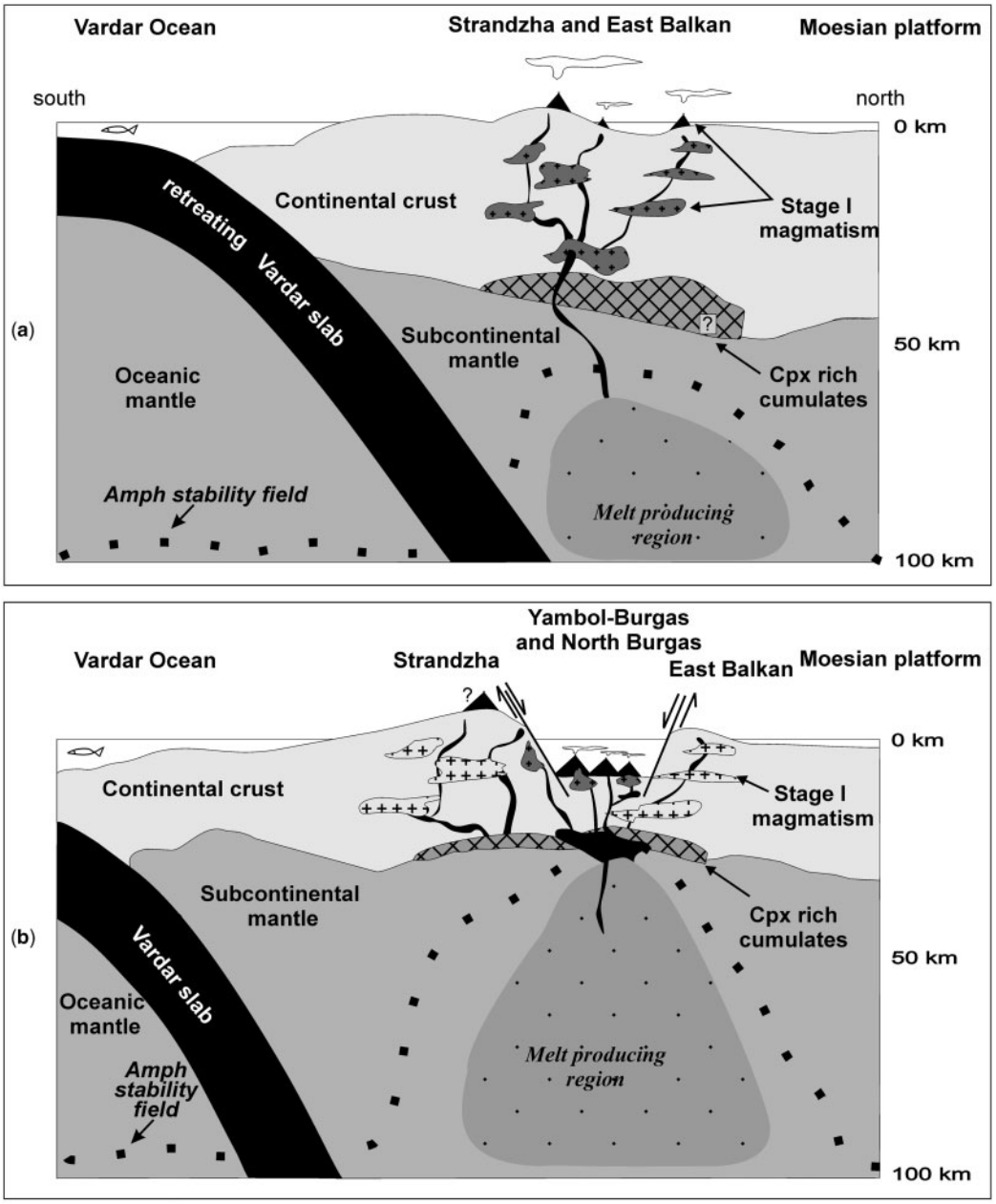

Fig. 18. Schematic illustration of the model for the evolution of magmatism in Eastern Srednogorie in the Late Cretaceous. (a) Normal subduction sequence with the formation of mostly tholeiitic and calc-alkaline intrusive rocks, shallow porphyries and volcanic rocks in present-day Strandzha and East Balkan region. (b) The Yambol–Burgas and North Burgas regions are formed as an intra-arc rift that split the former arc in two. Rifting resulted from slab retreat, break-off, or because of the continuing extension in the adjacent Black Sea basin, or some combination of these factors. The overall crustal thinning led to decompression of lower crustal or upper mantle amphibole-containing pyroxene-rich cumulates. Decompression, combined with increased heat flux from the increased corner flow of mantle material and the injection of mantle melts at the bottom of the crustal cumulates led to large-scale melting of clinopyroxene-rich material. Amphibole provided fluids, which further facilitated melting, as well as the alkalis for the high-K ankaramite volcanism in the Yambol–Burgas region. Fractional crystallization of the ankaramites in deep (equivalent to pressure of 8 kbar) magma chambers resulted in the formation of more evolved basalts and basaltic andesites.

not the dominant source for the magmatism in the area, either because wehrlite cumulates were absent in the lower crust of Strandzha, or because the thicker crust and/or overall compressional setting in this region prevented large-scale melting of such cumulates. Our data are the most compelling field-based evidence that nepheline-normative ankaramite magmas can form by remelting of lower crustal wehrlites, as previously indicated by thermodynamic modeling (Schiano *et al.*, 2000) and the experimental data of Médard *et al.* (2006), who interpreted the

presence of ankaramite melt inclusions and whole-rocks to reflect localized assimilative recycling of previous cumulates from the same volcanic edifice. Geochronology, geological evolution and temporally evolving Pb-isotope contrasts between magmas and xenoliths suggest a more limited role of such local assimilative recycling in the Eastern Srednogorie, and instead indicate a larger-scale two-stage process of early cumulate formation and subsequent remelting of lower crust in a tectonically evolving arc.

Mafic ankaramites from Lihir in the New Ireland region of eastern Papua New Guinea (Kennedy *et al.*, 1990) share common mineralogical and geochemical characteristics with the Eastern Srednogorie ankaramites. The Lihir lavas are clinopyroxene–olivine–plagioclase–Ti-magnetite- and apatite-containing silica-undersaturated, alkali-rich rocks, which have an arc-like trace-element signature and relatively unradiogenic Sr and Pb isotope compositions that show little variability. The two-stage model can also be applied to explain the formation of the Pliocene–Quaternary Lihir high-CaO rocks in a region with no active subduction or evidence for significant upper crustal contamination. The Middle Miocene subduction reversal in Papua New Guinea from a SSW to a NNE direction changed the tectonic setting in the area of Lihir from a forearc to a back-arc environment (Kennedy *et al.*, 1990). Similar to the slab roll-back induced intra-arc rift in the Yambol–Burgas region of Eastern Srednogorie, the tensional regime that followed in New Ireland led to progressive thinning of the crust (10–15 km present thickness) and the formation of fault-bounded sediment-filled stuctures along the length of the former arc. These geochemical and tectonic similarities to the Yambol–Burgas region may suggest a similar large-scale model for the formation of the Lihir alkaline arc lavas and the Eastern Srednogorie shoshonitic ankaramites, involving decompressional melting of former subduction-related amphibole-bearing clinopyroxenites in a tensional tectonic setting that followed calc-alkaline arc magmatism in New Ireland.

ACKNOWLEDGEMENTS

We thank Zhivko Ivanov, Stoimen Bilyarsky and Dimitar Paskalev for the assistance with the field work. This study represents part of S.G.'s PhD thesis in ETH Zurich supported by the Swiss National Science Foundation Projects No. 200020-100735, 200020-107955 and 200020-116693, which are gratefully acknowledged. We thank K. Panter, E. Médard and an anonymous reviewer for constructive comments and suggestions.

SUPPLEMENTARY DATA

Supplementary data for this paper are available at *Journal of Petrology* online.

REFERENCES

Aiello, E., Bartolini, C., Boccaletti, M., Gočev, P., Karagjuleva, J., Kostadinov, V. & Manetti, P. (1977). Sedimentary features of Srednogorie Zone (Bulgaria)—Upper Cretaceous intra-arc basin. *Sedimentary Geology* **19**, 39–68.

Allen, J. C., Boettcher, A. L. & Marland, G. (1975). Amphiboles in andesite and basalt. l. Stability as a function of P–T–fO_2. *American Mineralogist* **60**, 1069–1085.

Amov, B. & Arnaudov, V. (2000). Pb isotope data for Alpine magmatic rocks and related ore mineralizations in the Srednogorie metallogenic zone and Madan region in the Central Rhodope. In: *Abstracts of ABCD-GEODE Workshop*. Borovets, Bulgaria.

Antonijevic, I., Grubic, A. & Djordjevic, M. (1974). The Upper Cretaceous paleorift in Eastern Serbia. In: Janković, S. (ed.) *Metallogeny and Concepts of the Geotectonic Development of Yugoslavia, Belgrade, Faculty of Mining and Geology*, pp. 315–339.

Aoki, K.-I. & Shiba, I. (1973). Pyroxenes from lherzolite inclusions of Itinome-gata, Japan. *Lithos* **6**, 41–51.

Asimow, P. D., Dixon, J. E. & Langmuir, C. H. (2004). A hydrous melting and fractionation model for mid-ocean ridge basalts: Application to the Mid-Atlantic Ridge near the Azores. *Geochemistry, Geophysics, Geosystems* **5**, article number 01E16.

Bacon, C. R., Bruggman, P. E., Christiansen, R. L., Clynne, M. A., Donnelly-Nolan, J. M. & Hildreth, W. (1997). Primitive magmas at five Cascade volcanic fields: Melts from hot, heterogeneous sub-arc mantle. *Canadian Mineralogist* **35**, 397–423.

Banks, C. J. (1997). Basins and thrust belts of the Balkan Coast of the Black Sea. In: Robinson, A. G. (ed.) *Regional and Petroleum Geology of the Black Sea and Surrounding Region, AAPG Memoir* **68**, 115–128.

Banushev, B. (2003). Petrological characterisation of alkaline basaltoids from the region of St. Spas Bakadjik, Yambol district. *Annual of the University of Mining and Geology 'St. Ivan Rilski'* **46**, 13–18, (in Bulgarian).

Barsdell, M. & Berry, R. F. (1990). Origin and evolution of primitive island-arc ankaramites from Western Epi, Vanuatu. *Journal of Petrology* **31**, 747–777.

Benn, K., Nicolas, A. & Reuber, I. (1988). Mantle crust transition zone and origin of wehrlitic magmas—evidence from the Oman Ophiolite. *Tectonophysics* **151**, 75–85.

Berza, T., Constantinescu, E. & Vlad, S. N. (1998). Upper Cretaceous magmatic series and associated mineralisation in the Carpathian–Balkan Orogen. *Resource Geology* **48**, 291–306.

Boccaletti, M., Manetti, P. & Peccerillo, A. (1974). Hypothesis on plate tectonic evolution of Carpatho-Balkan Arcs. *Earth and Planetary Science Letters* **23**, 193–198.

Boccaletti, M., Manetti, P., A. Peccerillo, A. & Stanisheva-Vassileva, G. (1978). Late Cretaceous high-potassium volcanism in eastern Srednogorie, Bulgaria. *Geological Society of America Bulletin* **89**, 439–447.

Bončev, E. (1971). Lineamenttektonik und Schollengliederung der Erdkruste im ostlichen Teil der Balkanhalbinsel. *Annuaire de l'Université de Sofia, Faculté de Géologie et Géographie* **63**, 287–303.

Bonev, N. & Stampfli, G. (2008). Petrology, geochemistry and geodynamic implications of Jurassic island arc magmatism as revealed by mafic volcanic rocks in the Mesozoic low-grade sequence, eastern Rhodope, Bulgaria. *Lithos* **100**, 210–233.

Cheshitev, G. & Kanchev, I. (eds) (1989). *Geological Map of P. R. Bulgaria, 1:500 000*. Sofia: Supreme Technical Council.

Ciobanu, C. L., Cook, N. J. & Stein, H. (2002). Regional setting and geochronology of the Late Cretaceous Banatitic magmatic and metallogenetic belt. *Mineralium Deposita* **37**, 541–567.

Cioflica, G. & Vlad, S. (1973). The correlation of Laramian metallogenic events belonging to the Carpatho-Balkan area. *Revue Roumaine de Géologie, Géophysique et Géographie, Série de Géologie* **17**, 217–224.

Conrad, W. K. & Kay, R. W. (1984). Ultramafic and mafic inclusions from Adak Island–crystallization history, and implications for the nature of primary magmas and crustal evolution in the Aleutian Arc. *Journal of Petrology* **25**, 88–125.

Conrey, R. M., Sherrod, D. R., Hooper, P. R. & Swanson, D. A. (1997). Diverse primitive magmas in the Cascade arc, northern Oregon and southern Washington. *Canadian Mineralogist* **35**, 367–396.

Csontos, L. (1995). Tertiary tectonic evolution of the Intra-Carpathian area: a review. *Acta Volcanologica* **7**, 1–13.

Dabovski, C. (1991). Modern concepts on the evolution of the Alpine orogen in the Eastern Mediterranean and the Carpathian–Balkan area. A review and some problems of Bulgarian geotectonics. *Geotectonics, Tectonophysics and Geodynamics* **22**, 45–79.

Dabovski, C., Harkovska, A., Kamenov, B., Mavroudchiev, B., Stanisheva-Vassileva, G. & Yanev, Y. (1991). A geodynamic model of the Alpine magmatism in Bulgaria. *Geologica Balcanica* **21**, 3–15.

Dabovski, C., Boyanov, I., Khrischev, K., Nikolov, T., Sapounov, I., Yanev, Y. & Zagorčev, I. (2002). Structure and Alpine evolution of Bulgaria. *Geologica Balcanica* **32**, 9–15.

Dabovski, C., Kamenov, B. & Vassilev, E. (2009*a*). Upper Cretaceous magmatism. In: Zagorchev, I., Dabovski, C. & Nikolov, T. (eds) *Geology of Bulgaria. Volume II. Mesozoic Geology*. Sofia: Academic Publishing House 'Prof. Marin Drinov', pp. 423–553 (in Bulgarian).

Dabovski, C., Sinyovski, D., Vassilev, E. & Dimitrova, E. (2009*b*). Upper Cretaceous stratigraphy. In: Zagorchev, I., Dabovski, C. & Nikolov, T. (eds) *Geology of Bulgaria, Volume II. Mesozoic Geology*. Sofia: Academic Publishing House 'Prof. Marin Drinov', pp. 308–422, (in Bulgarian).

De Bari, S. M. (1997). Evolution of magmas in continental and oceanic arcs: The role of the lower crust. *Canadian Mineralogist* **35**, 501–519.

De Bari, S. M. & Coleman, R. G. (1989). Examination of the deep levels of an island-arc—evidence from the Tonsina ultramafic–mafic assemblage, Tonsina, Alaska. *Journal of Geophysical Research—Solid Earth and Planets* **94**, 4373–4391.

Della Pasqua, F. N. & Varne, R. (1997). Primitive ankaramitic magmas in volcanic arcs: A melt-inclusion approach. *Canadian Mineralogist* **35**, 291–312.

DePaolo, D. (1981). Trace elements and isotopic effects of combined wallrock assimilation and fractional crystallization. *Earth and Planetary Science Letters* **53**, 189–202.

Dewey, J., Pitman, W., Ryan, W. & Bonnin, J. (1973). Plate tectonics and the evolution of the Alpine system. *Geological Society of America Bulletin* **84**, 3137–3180.

Doglioni, C., Busatta, C., Bolis, G., Marianini, L. & Zanella, M. (1996). Structural evolution of the eastern Balkans (Bulgaria). *Marine and Petroleum Geology* **13**, 225–251.

Elburg, M., Kamenetsky, V. S., Nikogosian, I., Foden, J. & Sobolev, A. V. (2006). Coexisting high- and low-calcium melts identified by mineral and melt inclusion studies of a subduction-influenced syncollisional magma from South Sulawesi, Indonesia. *Journal of Petrology* **47**, 2433–2462.

Elburg, M. A., Kamenetsky, V. S., Foden, J. D. & Sobolev, A. (2007). The origin of medium-K ankaramitic arc magmas from Lombok (Sunda arc, Indonesia): Mineral and melt inclusion evidence. *Chemical Geology* **240**, 260–279.

Elliott, T. (2003). Tracers of the slab. In: Eiler, J. (ed.) *Inside the Subduction Factory. American Geophysical Union, Geophysical Monograph* **138**, 23–45.

Faure, G. & Mensing, T. (2005). *Isotopes—Principles and Applications*. New York: John Wiley.

Feig, S. T., Koepke, J. & Snow, J. E. (2006). Effect of water on tholeiitic basalt phase equilibria: an experimental study under oxidizing conditions. *Contributions to Mineralogy and Petrology* **152**, 611–638.

Foden, J. D. & Green, D. H. (1992). Possible role of amphibole in the origin of andesite—some experimental and natural evidence. *Contributions to Mineralogy and Petrology* **109**, 479–493.

Fügenschuh, B. & Schmid, S. M. (2005). Age and significance of core complex formation in a very curved orogen: Evidence from fission track studies in the South Carpathians (Romania). *Tectonophysics* **404**, 33–53.

Gasparon, M. & Varne, R. (1998). Crustal assimilation versus subducted sediment input in west Sunda arc volcanics: an evaluation. *Mineralogy and Petrology* **64**, 89–117.

Georgiev, G., Dabovski, C. & Stanisheva-Vassileva, G. (2001). East Srednogorie–Balkan rift zone. In: Ziegler, P. A., Cavazza, W., Robertson, A. H. F. & Crasquin-Soleau, S. (eds) *Peri-Tethys Memoir 6: Peri-Tethyan Rift/Wrench Basins and Passive Margins. Mémoires du Muséum d'Histoire Naturelle* **6**, 259–293.

Georgiev, S. (2008). Sources and evolution of Late Cretaceous magmatism in Eastern Srednogorie, Bulgaria: constraints from petrology, isotope geochemistry and geochronology. PhD thesis, ETH Zurich.

Georgiev, S. V., Von Quadt, A., Peytcheva, I., Marchev, P. & Heinrich, C. A. (2006). Eastern Srednogorie—new geochemical data for lateral zonation of magmatism. In: *Geosciences 2006*. Bulgarian Geological Society, Sofia, pp. 197–200.

Ghiorso, M. S., Hirschmann, M. M., Reiners, P. W. & Kress, V. C. (2002). The pMELTS: A revision of MELTS for improved calculation of phase relations and major element partitioning related to partial melting of the mantle to 3 GPa. *Geochemistry, Geophysics, Geosystems* **3**, article number 2001GC000217.

Gioncada, A., Clocchiatti, R., Sbrana, A., Bottazzi, P., Massare, D. & Ottolini, L. (1998). A study of melt inclusions at Vulcano (Aeolian Islands, Italy): insights on the primitive magmas and on the volcanic feeding system. *Bulletin of Volcanology* **60**, 286–306.

Green, D. H., Schmidt, M. W. & Hibberson, W. O. (2004). Island-arc ankaramites: Primitive melts from fluxed refractory lherzolitic mantle. *Journal of Petrology* **45**, 391–403.

Greene, A. R., DeBari, S. M., Kelemen, P. B., Blusztajn, J. & Clift, P. D. (2006). A detailed geochemical study of island arc crust: the Talkeetna Arc section, south–central Alaska. *Journal of Petrology* **47**, 1051–1093.

Gunn, B. M., Coyyll, R., Watkins, N. D., Abranson, C. E. & Nougier, J. (1970). Geochemistry of an oceanite–ankaramite–basalt suite from East Island, Crozet Archipelago. *Contributions to Mineralogy and Petrology* **28**, 319–339.

Günther, D., von Quadt, A., Wirz, R., Cousin, H. & Dietrich, V. J. (2001). Elemental analyses using laser ablation-inductively coupled plasma-mass spectrometry (LA-ICP-MS) of geological samples fused with $Li_2B_4O_7$ and calibrated without matrix-matched standards. *Mikrochimica Acta* **136**, 101–107.

Hart, S. R. (1984). A large-scale isotope anomaly in the Southern-Hemisphere mantle. *Nature* **309**, 753–757.

Hawkesworth, C. J., Gallagher, K., Hergt, J. M. & McDermott, F. (1993). Trace-element fractionation processes in the generation of island-arc basalts. *Philosophical Transactions of the Royal Society of London, Series A* **342**, 179–191.

Hill, R. E. T. & Boettcher, A. L. (1970). Water in Earth's mantle. Melting curves of basalt–water and basalt–water–carbon dioxide. *Science* **167**, 980–982.

Hoernle, K., Zhang, Y. S. & Graham, D. (1995). Seismic and geochemical evidence for large-scale mantle upwelling beneath the eastern Atlantic and Western and Central Europe. *Nature* **374**, 34–39.

Holloway, J. R. (1973). System pargasite–H_2O–CO_2—model for melting of a hydrous mineral with a mixed-volatile fluid. 1. Experimental results to 8 kbar. *Geochimica et Cosmochimica Acta* **37**, 651–666.

Holloway, J. R. & Burnham, C. W. (1972). Melting relations of basalt with equilibrium water pressure less than total pressure. *Journal of Petrology* **13**, 1–29.

Hsü, K., Nachev, I. & Vuchev, V. (1977). Geologic evolution of Bulgaria in the light of plate tectonics. *Tectonophysics* **40**, 245–256.

Hughes, C. J. (1982). *Igneous Petrology*. Amsterdam: Elsevier, 551 p.

Ivanov, R. (1979). To the tectonogeochemical analysis of the Upper Cretaceous magmatism in the East Srednogorie. *Review of the Bulgarian Geological Society* **40**, 47–61, (in Bulgarian, with English abstract).

Ivanov, Z. (1983). Aperçu géneral sur l'évolution géologique et structurale des Balcanides. In: *Livre–guide de l'excursion pour Réunion extraordinaire de la Société Géologique de France en Bulgarie*. Sofia: Société Géologique de Bulgarie, Press Universitaire, pp. 3–26.

Ivanov, Z. (1988). Aperçu géneral sur l'évolution géologique et structurale du massif des Rhodopes dans le cadre des Balkanides. *Bulletin de la Société Géologique de France*, **8**, IV, 2, pp. 227–240.

Jagoutz, O., Müntener, O., Ulmer, P., Pettke, T., Burg, J. P., Dawood, H. & Hussain, S. (2007). Petrology and mineral chemistry of lower crustal intrusions: the Chilas Complex, Kohistan (NW Pakistan). *Journal of Petrology* **48**, 1895–1953.

Janković, S. (1997). The Carpatho-Balkanides and adjacent area: a sector of the Tethyan Eurasian metallogenic belt. *Mineralium Deposita* **32**, 426–433.

Jenkins, D. M. (1983). Stability and composition relations of calcic amphiboles in ultramafic rocks. *Contributions to Mineralogy and Petrology* **83**, 375–384.

Kamenetsky, V. S., Eggins, S. M., Crawford, A. J., Green, D. H., Gasparon, M. & Falloon, T. J. (1998). Calcic melt inclusions in primitive olivine at 43°N MAR: evidence for melt–rock reaction/melting involving clinopyroxene-rich lithologies during MORB generation. *Earth and Planetary Science Letters* **160**, 115–132.

Kamenov, B., Tarassova, E., Nedialkov, R., Amov, B., Monchev, P. & Mavroudchiev, B. (2000). New radiometric data from Late Cretaceous plutons in the Eastern Srednogorie area, Bulgaria. *Geochemistry, Mineralogy and Petrology* **37**, 13–24.

Kawasaki, T. & Ito, E. (1994). An experimental determination of the exchange-reaction of Fe^{2+} and Mg^{2+} between olivine and Ca-rich clinopyroxene. *American Mineralogist* **79**, 461–477.

Kennedy, A. K., Hart, S. R. & Frey, F. A. (1990). Composition and isotopic constraints on the petrogenesis of alkaline arc lavas—Lihir Island, Papua New Guinea. *Journal of Geophysical Research—Solid Earth and Planets* **95**, 6929–6942.

Kersting, A. B. & Arculus, R. J. (1994). Klyuchevskoy volcano, Kamchatka, Russia—the role of high-flux recharged, tapped, and fractionated magma chamber(s) in the genesis of high-Al_2O_3 from high-MgO basalt. *Journal of Petrology* **35**, 1–41.

Kogiso, T. & Hirschmann, M. M. (2001). Experimental study of clinopyroxenite partial melting and the origin of ultra-calcic melt inclusions. *Contributions to Mineralogy and Petrology* **142**, 347–360.

Kouzmanov, K., Moritz, R., von Quadt, A., Chiaradia, M., Peytcheva, I., Fontignie, D., Ramboz, C. & Bogdanov, K. (2009). Late Cretaceous porphyry Cu and epithermal Cu–Au association in the Southern Panagyurishte District, Bulgaria: the paired Vlaykov Vruh and Elshitsa deposits. *Mineralium Deposita* doi:10,1007/s00126-009-0239-1.

Le Maitre, R. W., Bateman, P., Dudek, A., Keller, J., Lameyre, J., Le Bas, M. J., Sabine, P. A., Schmidt, R., Sorensen, H., Streckeisen, A., Woolley, A. R. & Zanettin, B. (1989). *A Classification of Igneous Rocks and Glossary of Terms*. Oxford: Blackwell.

Lilov, P. & Stanisheva-Vassileva, G. (1998). Exess ^{40}Ar, $^{87}Sr/^{86}Sr$ and K–Ar dating of minerals and rocks from the Tamarino paleovolcano. *Geochemistry, Mineralogy and Petrology* **33**, 61–72, (in Bulgarian, with English abstract).

Manetti, P., Peccerillo, A. & Poli, G. (1979). REE distribution in Upper Cretaceous calc-alkaline and shoshonitic volcanic rocks from Eastern Srednogorie (Bulgaria). *Chemical Geology* **26**, 51–63.

Marchev, P., Vaselli, O., Downes, H., Pinarelli, L., Ingram, G., Rogers, G. & Raicheva, R. 1998. Petrology and geochemistry of alkaline basalts and lamprophyres: implications for the chemical composition of the upper mantle beneath the Eastern Rhodopes (Bulgaria). In: Christofides, G., Marchev, P. & Serri, G. (eds) *Teriary Magmatism of the Rhodopian Region. Acta Vulcanologica* 10(2), 233–242.

Marchev, P., Georgiev, S., Zajacz, Z., Tommasini, S., Manetti, P. & von Quadt, A. (2007). High-K ankaramitic and high-Al magmas in the Eastern Srednogorie continental arc: Comparison between melt inclusion geochemistry and lavas. In: Moritz, R. and von Quadt, A. (eds) *Advances in Regional Geological and Metallogenic Studies in the Carpathians, Balkans, Rhodope Massif and Caucasus (Romania, Serbia, Bulgaria and Georgia)*. Field conference, September 4–7, 2007, Serbia. CD version.

Marchev, P., Georgiev, S., Zajacz, Z., Manetti, P., Raycheva, R., von Quadt, A. & Tommasini, S. (2009). High-K ankaramitic melt inclusions and lavas in the Upper Cretaceous Eastern Srednogorie continental arc, Bulgaria: Implications for the genesis of arc shoshonites. *Lithos* doi:10.1016/j.lithos.2009.03.14.

McCulloch, M. T. & Gamble, J. A. (1991). Geochemical and geodynamical constraints on subduction zone magmatism. *Earth and Planetary Science Letters* **102**, 358–374.

McKenzie, D. & O'Nions, R. K. (1991). Partial melt distributions from inversion of rare-earth element concentrations. *Journal of Petrology* **32**, 1021–1091.

McKenzie, D. & O'Nions, R. K. (1995). The source regions of ocean island basalts. *Journal of Petrology* **36**, 133–159.

Médard, E., Schmidt, M. W. & Schiano, P. (2004). Liquidus surfaces of ultracalcic primitive melts: formation conditions and sources. *Contributions to Mineralogy and Petrology* **148**, 201–215.

Médard, E., Schmidt, M. W., Schiano, P. & Ottolini, L. (2006). Melting of amphibole-bearing wehrlites: An experimental study on the origin of ultra-calcic nepheline-normative melts. *Journal of Petrology* **47**, 481–504.

Metrich, N. & Clocchiatti, R. (1996). Sulfur abundance and its speciation in oxidized alkaline melts. *Geochimica et Cosmochimica Acta* **60**, 4151–4160.

Metrich, N., Schiano, P., Clocchiatti, R. & Maury, R. C. (1999). Transfer of sulfur in subduction settings: an example from Batan Island (Luzon volcanic arc, Philippines). *Earth and Planetary Science Letters* **167**, 1–14.

Müntener, O., Kelemen, P. B. & Grove, T. L. (2001). The role of H_2O during crystallization of primitive arc magmas under uppermost mantle conditions and genesis of igneous pyroxenites: an experimental study. *Contributions to Mineralogy and Petrology* **141**, 643–658.

Mysen, B. O. & Boettcher, A. L. (1975). Melting of a hydrous mantle. 1. Phase relations of natural peridotite at high pressures and

temperatures with controlled activities of water, carbon dioxide, and hydrogen. *Journal of Petrology* **16**, 520–548.

Nachev, I. & Dimitrova, E. (1995*a*). Upper Cretaceous stratigraphy of the Eastern Balkan Mountains. *Geologica Balcanica* **25**, 43–74.

Nachev, I. & Dimitrova, E. (1995*b*). Upper Cretaceous stratigraphy of the Eastern Sredna Gora Zone. *Geologica Balcanica* **25**, 3–26.

Neubauer, F. (2002). Contrasting Late Cretaceous with Neogene ore provinces in the Alpine–Balkan–Carpathian–Dinaride collision belt. In: Blundell, D. J., Neubauer, F. & von Quadt, A. (eds) *The Timing and Location of Major Ore Deposits in an Evolving Orogen, Geological Society, London, Special Publication* **204**, 81–102.

Neumann, H., Mead, J. & Vitaliano, C. J. (1954). Trace-element variation during fractional crystallization as calculated from the distribution law. *Geochimica et Cosmochimica Acta* **6**, 90–100.

Nimis, P. (1995). A clinopyroxene geobarometer for basaltic systems based on crystal-structure modeling. *Contributions to Mineralogy and Petrology* **121**, 115–125.

Nimis, P. (1999). Clinopyroxene geobarometry of magmatic rocks. Part 2. Structural geobarometers for basic to acid, tholeiitic and mildly alkaline magmatic systems. *Contributions to Mineralogy and Petrology* **135**, 62–74.

Nimis, P. & Ulmer, P. (1998). Clinopyroxene geobarometry of magmatic rocks Part 1: An expanded structural geobarometer for anhydrous and hydrous, basic and ultrabasic systems. *Contributions to Mineralogy and Petrology* **133**, 122–135.

O'Hara, M. J. (1968). Bearing of phase equilibria studies in synthetic and natural systems on origin and evolution of basic and ultrabasic rocks. *Earth-Science Reviews* **4**, 69–133.

Okay, A., Satır, M., Tüysüz, O., Akyüz, S & Chen, F. (2001). The tectonics of the Strandja Massif: late-Variscan and mid-Mesozoic deformation and metamorphism in the northern Aegean. *International Journal of Earth Sciences* **90**, 217–233.

Pătraşcu, S., Bleahu, M., Panaiotu, C. & Panaiotu, C. E. (1992). The paleomagnetism of the Upper Cretaceous magmatic rocks in the Banat area of South Carpathians—tectonic implications. *Tectonophysics* **213**, 341–352.

Pătraşcu, S., Panaiotu, C., Seclaman, M. & Panaiotu, C. E. (1994). Timing of rotational motion of Apuseni Mountains (Romania)—paleomagnetic data from Tertiary magmatic rocks. *Tectonophysics* **233**, 163–176.

Pichavant, M., Mysen, B. O. & MacDonald, R. (2002). Source and H_2O content of high-MgO magmas in island arc settings: An experimental study of a primitive calc-alkaline basalt from St. Vincent, Lesser Antilles arc. *Geochimica et Cosmochimica Acta* **66**, 2193–2209.

Plank, T. (2005). Constraints from thorium/lanthanum on sediment recycling at subduction zones and the evolution of the continents. *Journal of Petrology* **46**, 921–944.

Plank, T. & Langmuir, C. H. (1998). The chemical composition of subducting sediment and its consequences for the crust and mantle. *Chemical Geology* **145**, 325–394.

Popov, P. (1981). Magmotectonic features of the Banat–Srednogorie Belt. *Geologica Balcanica* **11**, 43–72.

Popov, P. (1987). Tectonics of the Banat Srednogorie Rift. *Tectonophysics* **143**, 209–216.

Popov, P. (2002). Alpine geotectonic evolution and metallogeny of the eastern part of the Balkan Peninsula. *Annual of the University of Mining and Geology 'St. Ivan Rilski'* **45**, 33–38.

Popov, P., Bairaktarov, I. & Marinov, T. (1979). Magmatism and structure of the eastern part of the Burgas ore region I. Characterization of the magmatic formations. *Geologica Balcanica* **9**, 109–124.

Popov, P., Berza, T., Grubic, A. & Ioane, D. (2002). Late Cretaceous Apuseni–Banat–Timok–Srednogorie (ABTS) magmatic and metallogenic belt in the Carpathian–Balkan orogen. *Geologica Balcanica* **32**, 145–162.

Rickwood, P. C. (1989). Boundary lines within petrologic diagrams which use oxides of major and minor elements. *Lithos* **22**, 247–263.

Rollinson, H. (1993). *Using Geochemical Data: Evaluation, Presentation, Interpretation*. Essex: Longman Scientific & Technical.

Ruskov, K., von Quadt, A., Peytcheva, I., Georgiev, S., Strashimirov, S. & Stoykov, S. (2006). Geochemical and Sr–Nd isotope constraints on the Late Cretaceous magmatism in the area of the Zidarovo ore field. *Annual of the University of Mining and Geology 'St. Ivan Rilski'* **49**, 131–136.

Schiano, P. (2003). Primitive mantle magmas recorded as silicate melt inclusions in igneous minerals. *Earth-Science Reviews* **63**, 121–144.

Schiano, P., Eiler, J. M., Hutcheon, I. D. & Stolper, E. M. (2000). Primitive CaO-rich, silica-undersaturated melts in island arcs: Evidence for the involvement of clinopyroxene-rich lithologies in the petrogenesis of arc magmas. *Geochemistry, Geophysics, Geosystems* **1**, article number 1999GC000032.

Schmid, S., Bernoulli, D., Fügenschuh, B., Matenco, L., Schefer, S., Schuster, S., Tischler, M. & Ustaszewski, K. (2008). The Alpine–Carpathian–Dinaridic orogenic system: correlation and evolution of tectonic units. *Swiss Journal of Geoscience* **101**, 139–183.

Schmidt, M. W., Green, D. H. & Hibberson, W. O. (2004). Ultra-calcic magmas generated from Ca-depleted mantle: An experimental study on the origin of ankaramites. *Journal of Petrology* **45**, 531–554.

Smith, P. M. & Asimow, P. D. (2005). Adiabat_1ph: A new public front-end to the MELTS, pMELTS, and pHMELTS models. *Geochemistry, Geophysics, Geosystems* **6**, doi:10.1029/2004GC000816.

Spandler, C., Hermann, J., Arculus, R. & Mavrogenes, J. (2003). Redistribution of trace elements during prograde metamorphism from lawsonite blueschist to eclogite facies; implications for deep subduction-zone processes. *Contributions to Mineralogy and Petrology* **146**, 205–222.

Stampfli, G. M. & Borel, G. (2004). The TRANSMED transect in space and time: constraints on the paleotectonic evolution of the Mediterranean domain. In: Cavazza, W., Roure, F., Spakman, W., Stampfli, G. M. & Ziegler, P. (eds) *The TRANSMED Atlas: the Mediterranean Region from Crust to Mantle*. Berlin: Springer, pp. 53–90.

Stanisheva, G. (1969). Leucite basanites in the Tamarinski bakadjik, district of Jambol. *Comptes Rendus de l'Academie Bulgare des Sciences, Series II* **18**, 233–253, (in Bulgarian, with English abstract).

Stanisheva-Vassileva, G. (1980). The Upper Cretaceous magmatism in Srednogorie Zone, Bulgaria: a classification attempt and some implications. *Geologica Balcanica* **10**, 15–36.

Stanisheva-Vassileva, G. (1989). East Srednogorie volcano-intrusive area. In: Stanisheva-Vassileva, G., Strashimirov, S. & Yanev, Y. (eds) *Alpine Magmatism and Related Metallogeny in Srednogorie and Eastern Rhodopes—XIV Congress Carpatho-Balkan Geological Association, Sofia, Field Trip Guide Book*. Sofia: Sofia University, pp. 27–38 (in Russian).

Stanisheva-Vassileva, G. & Daieva, L. (1990). Across-arc geochemical variations of Late-Cretaceous magmatism in the Eastern Srednogorie, Bulgaria. *Geologica Balcanica* **20**, 78.

Stanisheva-Vassileva, G., Dabovski, C., Harkovska, A. & Stoyanov, S. (1994). 'Dike-in-dike complex' in Strandzha region (SE Bulgaria): implications on the Late Cretaceous subduction related magmatism. In: *Abstracts International Volcanological Congress, IAVCEI Ankara Ankara*. Ankara University.

Staudigel, H., Plank, T., White, B. & Schminke, H.-U. (1996). Geochemical fluxes during seafloor alteration of the basaltic upper oceanic crust: DSDP Sites 417 and 418. In: Bebout, G. E., Scholl, D. W., Kirby, S. H. & Platt, J. P. (eds) *Subduction: Top to Bottom. American Geophysical Union, Geophyical Monograph* **96**, 19–38.

Stracke, A., Hofmann, A. W. & Hart, S. R. (2005). FOZO, HIMU, and the rest of the mantle zoo. *Geochemistry, Geophysics, Geosystems* **6**, Q05007, doi:10.1029/2004GC000824.

Sun, S. S. & McDonough, W. F. (1989). Chemical and isotopic systematics of oceanic basalts: implications for mantle composition and processes. In: Saunders, A. D. & Norry, M. J. (eds) *Magmatism in the Ocean Basins. Geological Society, London, Special Publications* **42**, 313–345.

Tatsumi, Y. (2005). The subduction factory: how it operates in the evolving Earth. *GSA Today* **15**, 4–10.

Tatsumi, Y. & Eggins, S. (1995). *Subduction Zone Magmatism*: Blackwell, Oxford.

von Quadt, A., Ivanov, Z. & Peytcheva, I. (2001). The Central Srednogorie (Bulgaria) part of the Cu (Au-Mo) belt of Europe: A review of the geochronological data and the geodynamical models in the light of the new structural and isotopic studies. In: Piestrzyński, A. *et al*. (eds) *Mineral Deposits at the Beginning of the 21st Century, Proceedings of the Joint Sixth Biennial SGA–SEG Meeting, Krakow, Poland, 26–29 August 2001.* Krakow: A. A. Balkema, pp. 555–558.

von Quadt, A., Moritz, R., Peytcheva, I. & Heinrich, C. A. (2005). Geochronology and geodynamics of Late Cretaceous magmatism and Cu–Au mineralization in the Panagyurishte region of the Apuseni–Banat–Timok–Srednogorie belt, Bulgaria. *Ore Geology Reviews* **27**, 95–126.

Workman, R. K. & Hart, S. R. (2005). Major and trace element composition of the depleted MORB mantle (DMM). *Earth and Planetary Science Letters* **231**, 53–72.

Yosifov, D. & Pchelarov, V. (1977). A scheme of the thickness of the Earth's crust in the Balkan Peninsula and some features of its structures. *Geologica Balcanica* **7**, 7–22 (in Russian, with English abstract).

Zimmerman, A., Stein, H. J., Hannah, J. L., Kozelj, D., Bogdanov, K. & Berza, T. (2008). Tectonic configuration of the Apuseni–Banat–Timok–Srednogorie belt, Balkans–South Carpathians, constrained by high precision Re–Os molybdenite ages. *Mineralium Deposita* **43**, 1–21.

Zindler, A. & Hart, S. (1986). Chemical geodynamics. *Annual Review of Earth and Planetary Sciences* **14**, 493–571.